Westerduinweg 3
1755 LE Petten
P.O. Box 15
1755 ZG Petten
The Netherlands

www.tno.nl

T +31 88 866 50 65

TNO report

TNO 2020 R11300

AWC validation methodology

Date	August 2020
Author(s)	S. Kanev
Copy no	
No. of copies	
Number of pages	58 (incl. appendices)
Number of appendices	0
Sponsor	PPS-toeslag TKI-Energie
Project name	Dynamic Robust Wind Farm Control (DySCon)
Project number	060.40694

Revision history

Rev.	Date	Description
1	06-2020	AWC validation method described
2	27-8-2020	First draft of complete report
3	1-9-2020	Update after internal review by D. Wouters

Summary

This report describes a validation methodology for active wake control (AWC) by wake redirection, a wind farm operation strategy aiming to increase the overall power production of the wind farm. The power gain is achieved by reducing wake effects through intentional yaw misalignment of the rotors of upstream wind turbines to change the path of the wakes and avoid impinging on downstream turbines.

The AWC validation methodology, described here, complies with the agreed requirements, and details on the following aspects:

- determination of reference wind velocity using nacelle anemometry
- determination of reference wind direction using nacelle anemometry
- data filtering and data binning
- dealing with turbine unavailability, curtailment and power-boosting
- calculation of power ratio per bin and overall, including relevant statistics
- impact of the choice of the toggle period on the accuracy of the results
- uncertainty assessment

A number of examples using real life data from several wind farms is used to illustrate the most important components of the AWC validation methodology. Still, at the point of preparing this document, no data is yet available from actual full-scale field tests with AWC by yaw redirection, and therefore the method could not yet be fully tested. This is planned to be done in the near future.

This work is carried out in the framework of the project Dynamic Robust Wind Farm Control (DySCon), which is partially funded by the TKI Wind op Zee PPS-toeslag program of the Dutch Ministry of Economic Affairs. This document represents Deliverable D5 “Written report describing the AWC validation methodology”.

Contents

1 Introduction

Active Wake Control (AWC) comprises a family of methods for operating wind farms in such a way as to mitigate the wake effects on the downstream wind turbines, namely the wake losses and structural loading. At present, there are two concepts to AWC that are of practical relevance. The first one, induction control, relies on controlling the axial induction of the rotor of upstream wind turbines to increase the wind velocity in the wake, ideally achieved by increasing the pitch angle at below rated wind conditions. The second AWC concept, wake redirection, requires operating upstream turbines with intentional yaw misalignment to move the wake away from downstream wind turbines. Both methods sacrifice some power production upstream to enable downstream turbines to produce more power and increase the overall wind farm power production.

Even though the wake redirection concept is seen as more hazardous as operation with intentional misalignment is not a condition current wind turbines are designed to operate in, this method is shown in many recent simulation studies to bring a much more significant power increase than induction control. Some recent field studies have confirmed the potential benefits of wake redirection in limited scale experiments with up to a few wind turbines. The next step in maturing the technology is to demonstrate the added value in a full-scale setting with the first generation commercial AWC software. Such tests are planned to be carried out by SGRE in two pilot projects at commercial offshore wind farms.

In order to be able to assess the actual upside from AWC in the field, a proper method for the analysis of the actual benefits in terms of energy yield increase from AWC needs to be in place. The development of such AWC validation methodology is the topic of this work. The validation methodology includes a method with a measurement campaign involving the available on-site measurement equipment only. Even though the validation methodology is specifically developed for AWC by wake redirection control, it can readily be applied to induction control with small modifications.

This document continues by describing the requirements that were posed on the AWC validation methodology, then lists the challenges that need to be addressed, and subsequently details the different components of the proposed methodology for assessment of the power production benefit from AWC. Numerous examples with real-life measurement data are included to illustrate specific topics, but an overall application of the developed methodology to an actual full-scale AWC test campaign has not yet been carried out due to lack of experiment. The AWC validation methodology is planned to be applied to data from above-mentioned SGRE AWC pilot projects.

2 Requirements on the validation methodology

The AWC validation methodology should be widely applicable and not be restricted to specific sites or measurement equipment. The following list of requirements on the AWC validation methodology has been agreed with project partner SGRE:

- Applicable to large offshore wind farms of *any* layout.
- Shall not assume availability of historic data.
- Will include a method with a measurement campaign involving the available on-site measurement equipment only.
- Measurement data: standard SCADA 10-min data or faster, if necessary.
- No simulation models to be used to fill in missing data in the measurements.
- (soft requirement) Ideally, the maximum duration of the trials is one year. It might possibly consist of a number of shorter periods of several months, with the accuracy increasing after each period.

3 Challenges to address

Based on the requirements for the validation methodology, set out in the previous chapter, a set of research questions is defined here. These questions represent the challenges that need to be properly addressed to ensure that validation methodology complies with the posed requirements. These challenges are subsequently addressed in detail in the next section.

1. How to determine the wind velocity using nacelle anemometry?
   The transfer function of the nacelle-based anemometer is expected to be affected by yaw misalignment. In order to be able to compare power production data from nominal and test cases, it is imperative to have consistent wind speed measurements throughout the whole test campaign.
2. How to determine the wind direction using nacelle anemometry?
   There are two sources of concern here. Firstly, the wind direction measurement may be biased under yaw misalignment. Secondly, the nacelle direction sensor may exhibit occasional jumps or drifts.
3. What filtering should be applied to the data?
   Power production, curtailment, power boosting, data quality (outliers).
4. How to bin the data to ensure sufficient number of data points in each bin?
   Binning will have to be applied not only to the wind speed, but also to the wind direction. This can easily result in a large number of bins with insufficient number of points within some bins, and therefore large uncertainty. Too large bins, on the other hand, can affect the accuracy of the AWC validation method since the variation of the power gain by AWC within a bin can be rather large.
5. How to deal with turbine unavailability, curtailment and power-boosting?
   The percentage of time that all turbines are available is lower than the single turbine availability. SCADA data can also show periods of unavailability even when turbines are in operation. Filtering out data during periods of unavailability of (data from) any turbine in the farm might be too restrictive in terms of required duration of the test campaign.
6. Do we need to include information about the atmospheric conditions in the analysis (e.g. corrections for air density, TI) and, if so, how to determine these?
   The power performance measurements standard IEC 61400-12-1 [1] describes the normalizations that need to be applied to air density, turbulence intensity and wind shear. These are meant to enable the comparison of results from different data sets bringing them to a similar scale.
7. How to calculate the relative power gain, within each bin and on an yearly basis?
8. How should the toggling between nominal and test cases be performed?
   The generic layout requirement essentially excludes the possibility for side-by-side testing.
9. What is the uncertainty on the relative power increase?
   Proper uncertainty analysis is essential in providing good understanding of the accuracy of the calculated power gain.

4 AWC validation approach

This chapter describes the proposed AWC validation methodology. By addressing the challenges listed in chapter 3 one by one, a collection of procedures and recommendations is derived that constitutes the validation methodology.

4.1 Determination of the wind velocity using nacelle anemometry

The requirements for using only the available measurement equipment at the test site stipulate that the methodology should be applicable even when the free stream conditions are not measured directly. Therefore, only the conventionally available nacelle based measurement of the wind velocity will be used. This measurement is behind the rotor, being disturbed by the rotor blades, hub and nacelle.

The IEC 61400-12-2:2013 [2] standard provides a methodology for power performance measurement of a stand-alone wind turbine using nacelle anemometry. The methodology stipulates the construction of the so-called nacelle transfer function (NTF), describing the relationship between the measured wind speed on the nacelle and the free stream velocity. When unavailable, this NTF is to be constructed using metmast measurements. To this end, the conventional binning approach is used with linear interpolation between bins. When provided, the NTF must be checked for validity.

Since not every offshore wind farm contains a metmast, no availability of metmast measurements can be assumed in the AWC validation methodology. This means that it will not be possible to establish the NTF relationship using measurement data. It can also not be assumed that an NTF will be provided by the turbine manufacturer.

The above implies that the AWC validation methodology should not use the free wind velocity as there might be no reliable way for deriving it accurately from the nacelle-based wind speed measurements. This, by itself, is not necessarily a problem as long as nacelle-based wind velocity measurements can be used which are consistent during operation under different yaw misalignments. After all, the purpose of the AWC validation approach is to determine the power production increase by AWC, and not to calculate a power curve.

Clearly, the wind speed measurement on the nacelle will be biased by the yaw misalignment. Indeed, the nacelle-based wind speed and wind direction measurements are influenced by the rotor wake [3], the characteristics of which change with yaw misalignment. Therefore, it will be necessary to establish a relationship between the nacelle-based wind speed measurement during operation with yaw misalignment and that during nominal operation without yaw offset. This relationship will be called here wind speed transfer function (WSTF). When not available, the WSTF will have to be established experimentally for a set of different yaw misalignment angles covering the complete range of yaw misalignments expected during AWC operation. When the WSTF is provided, it needs to be checked for validity. To this end, the construction of the WSTF needs to have been carried out on the same turbine type, equipped with the same hardware and software, and at similar site conditions, and has to be reported in such detail that the derived transfer function relations can be properly verified.

To construct the WSTF, measurement data needs to be collected by at least one turbine operating with intentional yaw misalignment and at least one neighbouring turbine operating nominally, where both turbines operate in free stream. These measurement data can often be collected in parallel with the actual AWC validation tests,

since AWC is typically only active within certain wind direction sectors. Outside these sectors AWC will not be active, and the free stream wind turbines could be used to construct the WSTF. This will require to operate some of the free stream turbines with intentional yaw misalignment while the other free stream turbines are operated nominally. The WSTF can then be constructed in a similar manner as the conventional NTF is constructed according to IEC 61400-12-2, with the difference that the metmast measurement required in the mentioned standard is now replaced with (possibly a combination of) the nacelle-based measurement(s) at the nominally operated wind turbine(s). This way the WSTF will represent the transfer function between the nacelle-based wind speed measurement at a misaligned turbine and that at a turbine operated nominally. This process will need to be repeated for different yaw misalignment angles, so that the final WSTF will constitute a set of transfer functions.

The so-constructed WSTF will be used to correct the wind velocities measured at the yawed turbines during the AWC experiments, making them more consistent with the reference measurements without yaw misalignment.

Example 1 (NTF for different yaw offsets)

Within the EU H2020 project Closed-loop wind farm control (CL-Windcon), experiments were performed on a GE 1.5 MW wind turbine that was operated with intentional yaw misalignments varying between −20° and 20°. The duration of the campaign was four months, during which period the yaw offset setpoints were periodically toggled. From the data made available, the following data is used in the example here:

- *1-minute averaged operational SCADA data from the test turbine, including power production, wind speed, yaw error, nacelle position, rotor speed, pitch angle, and target yaw misalignment angle.*
- *1-min wind measurement data at a metmast located at a distance of just 100 m from the test turbine. The metmast has been properly calibrated prior to the tests, and the wind speed and wind direction measurements at height 61.5 m (close to the hub height of 65 m) are used here.*
- *1-min measurements from an iSpin spinner anemometer mounted on the hub of the test turbine, including wind speed, yaw offset and nacelle direction (measured using a magnetic compass).*

Since there were no data available from neighbouring wind turbines operating nominally (without intentional yaw misalignment), this example uses the metmast measurements instead. Therefore, it will be the NTF that will be estimated here (as defined in IEC 61400-12-2), rather than the WSTF defined above. However, instead of a single NFT, a set of NTFs will be constructed, each representative for one yaw misalignment angle. This way we can study the impact of yaw misalignment on the bias of the nacelle-based wind speed measurements, and demonstrate the proposed mechanism for correcting these.

A complication in the analysis of these field data was that none of the available sensors could provide an accurate and reliable measurement of the actual yaw error. The available yaw sensor on the nacelle was considered not reliable enough for the purpose here due to occasional jumps that it exhibited. The iSpin measurement was found to be stable and reliable, but seemed to overestimate the actual yaw offsets (this will be illustrated later on in Example 3). For this reason, it was decided to calculate the yaw error as the difference between the wind direction measurement at the metmast and the nacelle position measurement. Due to jumps and drifts in the

internal nacelle heading sensor, it was decided to use the iSpin magnetic compass as measurement of the nacelle direction. Before doing that, however, a software calibration was performed on the iSpin compass measurement by using only data during operation without intentional yaw misalignment. To this end, a calibration constant is calculated as follows

$$C_{compass} = \alpha^{avg}_{yaw,iSpin} - \left(\alpha^{avg}_{nac,iSpin} - \alpha^{avg}_{wd,MM}\right) \tag{4.1}$$

wherein $\alpha^{avg}_{yaw,iSpin}$ is the average yaw offset measured by the iSpin, $\alpha^{avg}_{nac,iSpin}$ is the average nacelle heading measurement by the iSpin compass, and $\alpha^{avg}_{wd,MM}$ is the average wind direction measurement at the metmast. Notice that $\alpha^{avg}_{yaw,iSpin}$ also represents the iSpin estimate of the static yaw misalignment angle of the nacelle under normal operation (without intentional misalignment), which for the illustration purpose of this example is assumed accurate enough as this is the primary function of this device. The calibrated yaw error $\alpha_{yaw,clbr}$ is then the difference between the calibrated nacelle heading measurement by the iSpin compass, $\alpha_{nac,iSpin} + C_{compass}$, and the wind direction measurement at the metmast $\alpha_{wd,MM}$:

$$\alpha_{yaw,clbr} = (\alpha_{nac,iSpin} + C_{compass}) - \alpha_{wd,MM}. \tag{4.2}$$

The following steps were taken to perform the analysis in this example:

- *The available 1-min data is filtered, retaining only data from free stream operation of the test turbine, while operating in power production mode. Obvious outliers are removed as well.*
- *The calibrated yaw error $\alpha_{yaw,clbr}$ is calculated as outlined above.*
- *A set of yaw errors was selected at which the NTF is to be constructed: −20°, −10°, 0°, 10° and 20°. For a given yaw error bin, the following processing is performed:*
  - *Data is filtered, retaining only data samples for which the calibrated yaw offset lies within 5 degrees of the given yaw error bin centre.*
  - *The nacelle-based wind speed measurements are binned, and for each bin the corresponding metmast wind speed measurements are averaged. This binning yields the NTF for the given yaw error bin, relating the nacelle-based wind speed measurements to the metmast ones by means of piecewise linear functions. For instance, the NTF computed for a yaw offset of −20° is depicted by the red line in Figure 1. It should be pointed out that, besides the binning approach, other approaches to modelling this relationship have been investigated, but none of them was able to deliver a noticeable improvement over the binning approach. These approaches were linear least squares fitting on the raw wind speed data (black line in Figure 1), and weighted linear least squares fitting on the binned wind speed data with weights inversely proportional to the square errors in each bin (blue line in Figure 1).*
- *The accuracy of the NTF approach is verified by analysing the difference between the metmast wind speed measurement and the nacelle-based wind speed measurement (original versus calibrated through the NTF). The calibrated nacelle-based wind speeds are computed by 2-dimensional linear interpolation of the NTF data, the dimensions being the uncalibrated nacelle-based wind velocity and the calibrated yaw offset. The mean difference per yaw offset is depicted in Figure 2. The figure shows a clear trend in the uncalibrated (raw) wind speed measurement error on the nacelle as function of the yaw offset. After calibration through interpolation using the*

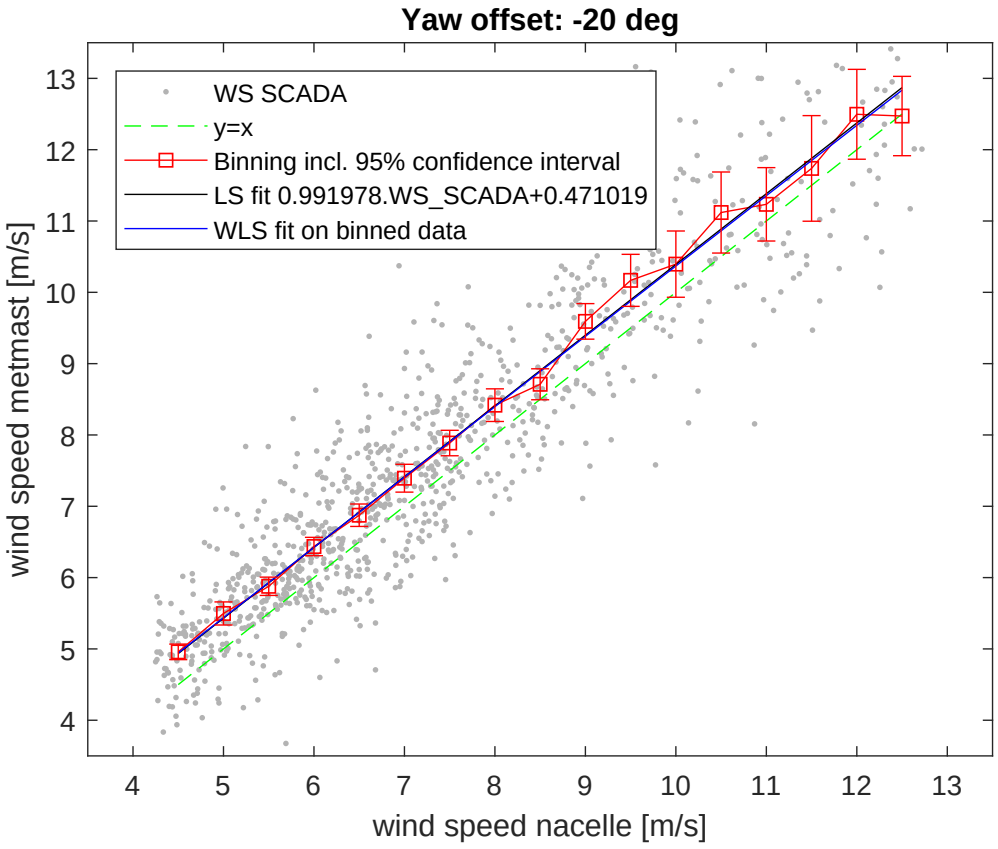

Figure 1: Example of NTF for yaw offset of −20°

NTF, the difference between the metmast and nacelle-based measurements significantly decreases, and no trend with the yaw offset is observed any more.

Now that there is an approach to properly derive consistent nacelle-based wind speed measurements, compensating for the effect of yaw misalignment, one single wind velocity signal representative for the whole wind farm will have to be constructed. This signal will be called “consensus wind speed”, V_{cons}, and will be used in the process of binning, discussed in section 4.4. For obvious reasons it makes sense to calculate V_{cons} as the average value of the wind speed measurements at all wind turbine operating in free stream. Unavailable, or non-operational wind turbines should be excluded. In order to determine which turbines are in free stream operation, the farm-average nacelle-based wind direction measurement can be used in combination with a simple but conservative wake expansion model, such as the Jensen model:

$$w\left(x\right) = k_w.x + D. \tag{4.3}$$

Here $w\left(k\right)$ is the wake width at distance x downstream, D is the rotor diameter, and k_w is the wake expansion constant. A value $k_w = 0.065$ is recommended.

4.2 Determination of the wind direction using nacelle anemometry

Similar argumentation to that used in the previous section for the wind speed measurement is applicable to the wind direction measurement. The requirements for using the available measurement equipment at the test site only stipulates that the methodology should be applicable even when the free stream direction is not measured directly. Therefore, the conventionally available nacelle position measurement,

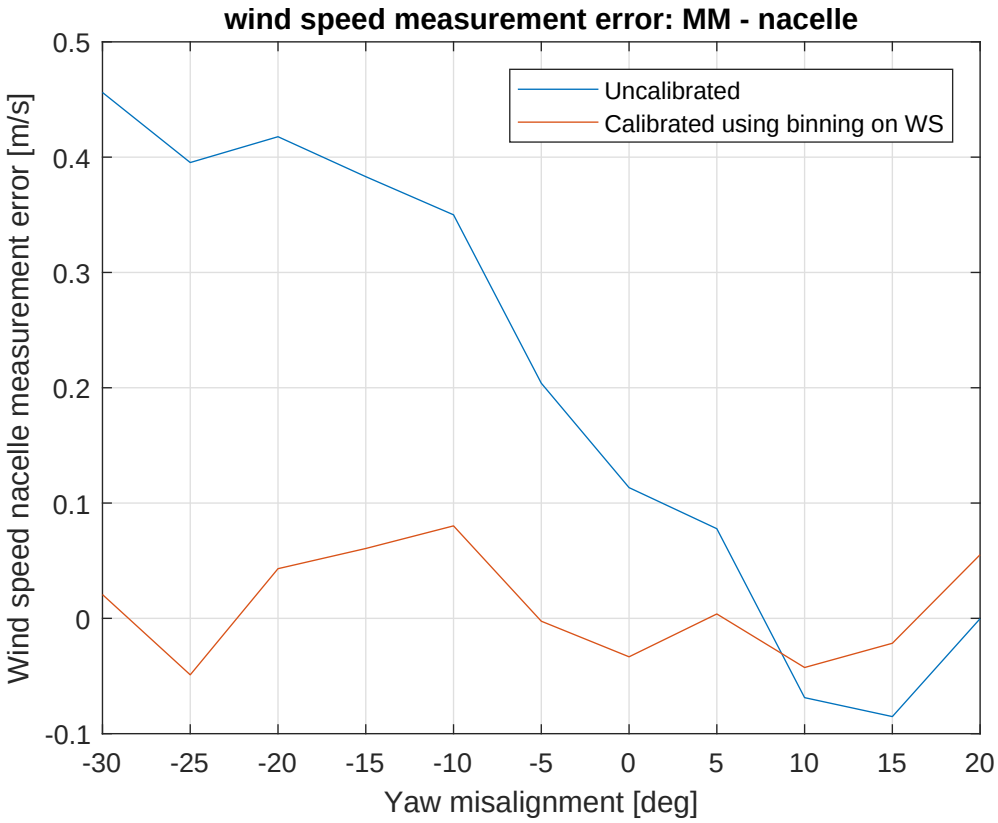

Figure 2: Mean error between the wind speed measurement at the metmast and the nacelle

in combination with the yaw error measurement (i.e. nacelle-based relative wind direction), will have to be used to construct true wind direction measurement. The yaw error measurement is behind the rotor, being disturbed by the rotor blades, hub and nacelle.

Since the yaw error measurement can get biased under operation with intentional yaw misalignment [3], it will be important to establish the relationship between the wind direction measurement during intentional misalignment and that during nominal operation. This relation will be called here the wind direction transfer function (WDTF). The WDTF should be constructed (when not available), or checked for validity (when provided). For validity check, the construction of the WDTF needs to have been carried out on the same turbine type, equipped with the same hardware and software, and at similar site conditions, and has to be reported in such detail that the derived transfer function relations can be properly verified.

To construct the WDTF, measurement data needs to be collected by at least one turbine operating with intentional yaw misalignment and at least one neighbouring turbine operating nominally, where both turbines operate in free stream. These measurement data can often be collected in parallel with the actual AWC validation tests, since AWC will typically operate within certain wind direction sectors. Outside these sectors AWC will not be active, and the free stream wind turbines can be used for experiments for constructing the required WDTF. These experiments will require to operate some of the free stream turbines with yaw misalignment while the other free stream turbines are operated nominally. Notice also that the construction of the WDTF and the WSTF can be performed using the measurement data from the same experiment.

As pointed out above, the true wind direction is not directly measured. Instead, it is

constructed using measurements of the nacelle position and the yaw error. At present, the conventional nacelle direction measurements are only used for monitoring the cable twisting in order to activate the untwisting sequence when necessary. Typically, this process does not require precise measurement of the nacelle orientation with respect to the true North. Because of that, the currently used nacelle direction sensors are often biased. In some systems, this bias is even varying with time, exhibiting drifts and/or abrupt changes.

For the proper operation of AWC, high accuracy wind direction measurements need to be in place. Therefore, it can be expected that the nacelle direction measurements would have been properly calibrated before the actual start of the AWC measurement campaign. As long as the wind direction measurements remain consistent in time, the AWC validation methodology does not require high accuracy calibration with respect to true North. However, since the nacelle position measurement are known to exhibit a time varying bias in some commercial turbines, a calibration methodology will be developed here to enable possible re-calibration during the AWC test campaign, if necessary.

Therefore, the following steps will be required to ensure that a reliable and consistent wind direction estimate will be available for AWC validation:

1. Calibration of the nacelle direction measurements to remove constant biases, at least for the turbines located on the edge of the wind farm. This can be achieved by means of power deficit analysis using data from nominal operation without intentional misalignment. This calibration could use either recent historical data, or newly collected data from the AWC validation campaign. Although not strictly required for the AWC validation, calibration can also be performed on the nacelle direction measurements at the inner wind turbines using the averaged calibrated wind direction at the outer turbines.
2. Construction of the WDTF using measurement data collected during operation with intentional misalignment. For this step, data is required from at least two neighbouring wind turbines, both operating in free stream, but only one of them operating with intentional yaw misalignment. The intentional yaw misalignment setpoint should also be varied to cover the complete range of yaw misalignment setpoints expected to occur during AWC operation. Alternatively, a provided WDTF could be used after it has passed the check for validity, outlined in the beginning of this section.
3. Using the WDTF to apply correction on the measured wind direction during operation with intentional yaw misalignment to ensure consistency with the measurements under nominal operation.
4. Constructing a single consensus wind direction measurement by averaging the corrected wind direction measurements at the upstream wind turbines operating in free stream conditions, to be used for binning (section 4.4).

These steps will be illustrated below in two examples. First, in Example 2, the calibration of the nacelle direction measurement will be discussed. Subsequently, due to the lack of data for proper illustration of the construction of the WDTF, Example 3 will be limited to showing the effect of yaw misalignment on the yaw error measurement.

Example 2 (Calibration of nacelle direction measurements)

In this example, SCADA data from offshore wind farm Gwynt y Mor is used. The data is collected over a period of two years (Nov'17 to Nov'19). The data includes

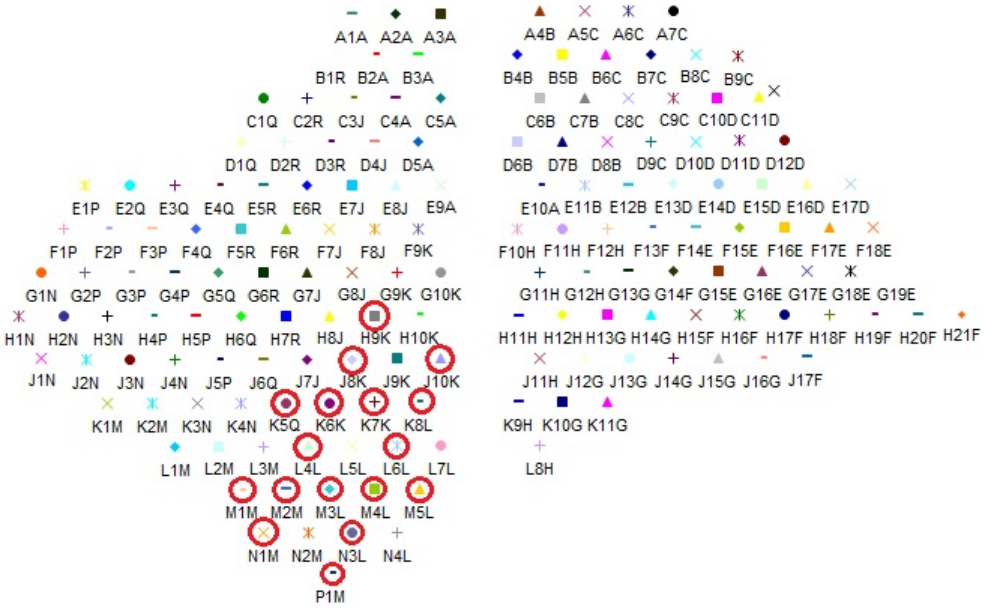

Figure 3: Layout of the Gwynt y Mor wind farm

10-min operational data for 17 of the 160 wind turbines at Gwynt y Mor. These turbines are encircled in the layout plot in Figure 3. All turbines are of the type Siemens SWT-3.6-107, i.e. 3.6 MW with 107 m rotor diameter.

To illustrate the offset (bias) in the nacelle direction measurements, Figure 4 is provided depicting these measurements at the different wind turbines over a period of one week. Clearly, there is a significant bias present, which is a common phenomenon in the current wind turbines. Luckily, this bias is not varying significantly with time for this wind turbine type and can be removed relatively simply, as will be illustrated in this example.

The nacelle direction measurement offsets can be estimated using power measurements in combination with the turbine coordinates. The idea behind this approach is to calculate the power ratio between the measured power production of the to-be-calibrated turbine and another (ideally adjacent) turbine, both operating in partial load. This power ratio should have a dip centred around the wind direction aligned with the two turbines. The nacelle direction reading can then be calibrated to achieve this condition. Clearly, within a wind farm the power ratio between any two turbines will have different dips at different wind directions, depending on the layout, as illustrated in Figure 5. The blue dots in the figure depict the ratio between the power production measured at turbine N3L and that at turbine P1M, expressed versus the wind direction at N3L. As the focus lies on the dips in the power ratio, only values in the interval [0, 1.4] are plotted. Also, due to the fact that no yaw error measurement data was available, the wind direction was approximated by the measured nacelle orientation in this example. Due to the location of N3L with respect to the other turbines, there are several significant power dips observable, which complicates the determination the proper calibration offset.

The calibration is significantly simplified if a wake model is used in combination with the measurement data. The red line in Figure 5 represents the modelled ratio computed using the FarmFlow wake model [4]. The nacelle direction measurement at N3L can then be calibrated, for instance, by using least squares fitting of the raw data to the model. That way, a calibration offset of −8° was computed for turbine N3L.

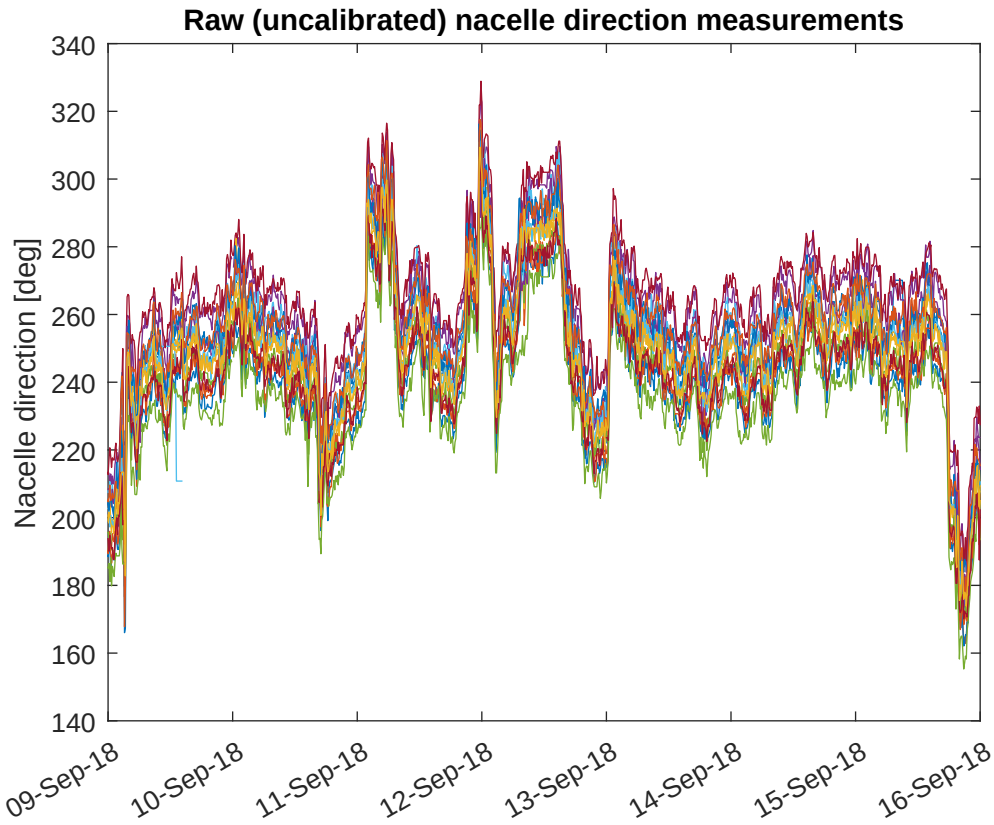

Figure 4: One week of raw nacelle direction measurements

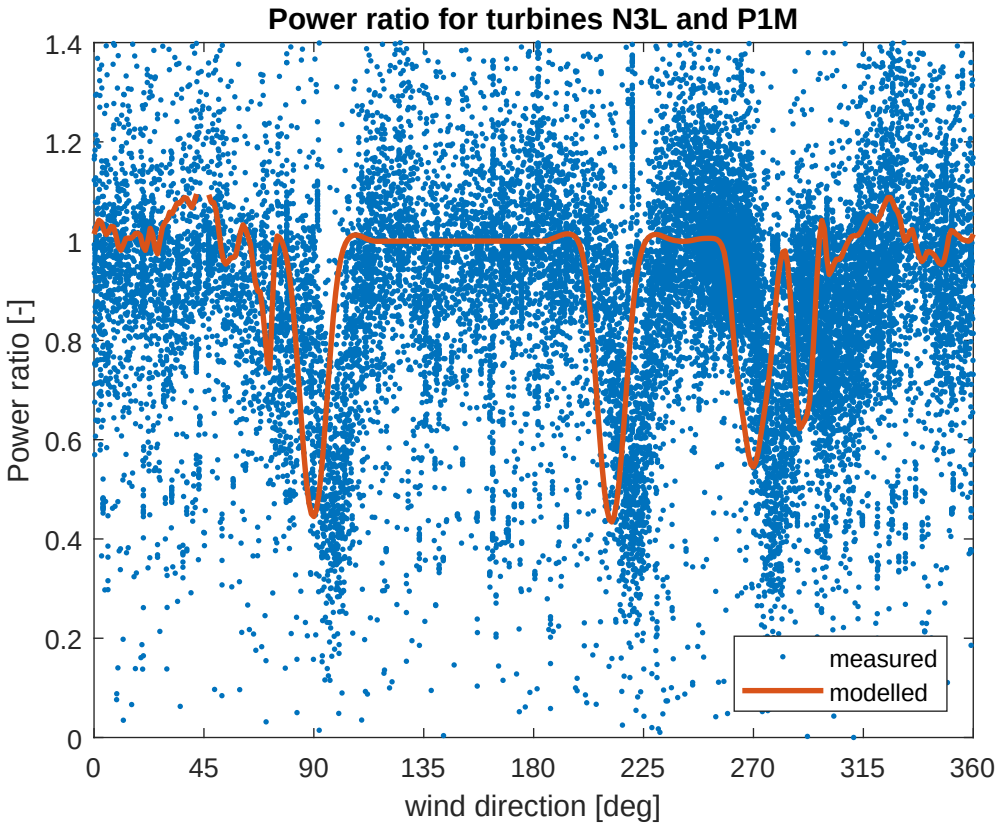

Figure 5: Power ratio between turbines N3L and P1M

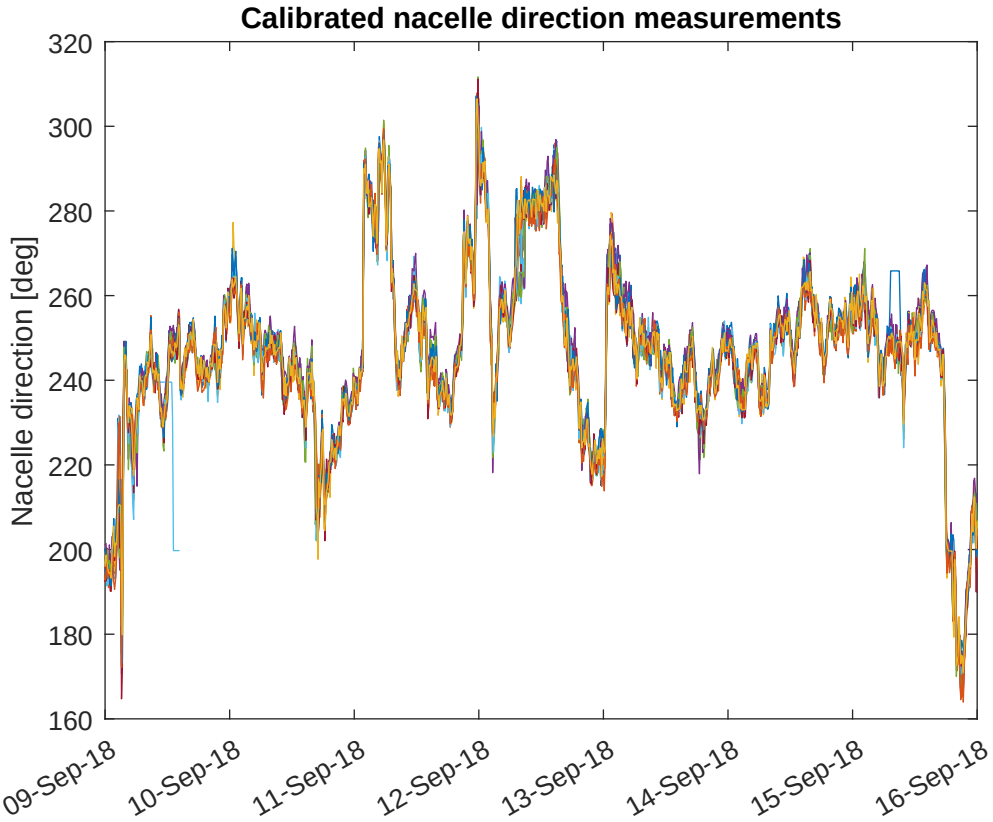

Figure 6: One week of calibrated nacelle direction measurements

To improve the calibration accuracy even further, power ratios between a to-be-calibrated turbine (say P1M) and a number of adjacent turbines (say M1M, M2M, M3M, M4L, M5L, N1M, N3L) can be used. In doing so, however, the following quality assurance criteria are used in this example to ensure high accuracy calibration results:

- *Turbines beyond the first two turbines downstream are excluded. The reason for this is that in multiple wake situations the power ratio data gets too scattered and deteriorates the estimation accuracy.*
- *Turbines in the far wake of the turbine being calibrated (at a distance of, say, more than 20 D) are excluded. The power deficit is not sufficiently well pronounced at such distances.*
- *The power ratio analysis is only performed for pairs of turbines for which the number of significant power deficit dips (lower than 0.8) is not too large. The reason for this is that, when there are too many power dips, the calibration approach becomes poorly conditioned and can lead to convergence to a wrong calibration offset.*
- *After the power deficit based calibration process is completed for all turbines, an accuracy quality check is applied to validate the accuracy of the calibration. The calibration is undone for those turbines that do not pass the accuracy quality test, meaning that the calibrated nacelle measurement should not deviate by more than 1° from the average nacelle direction value (the average is evaluated on the circle and using only the calibrated measurements).*

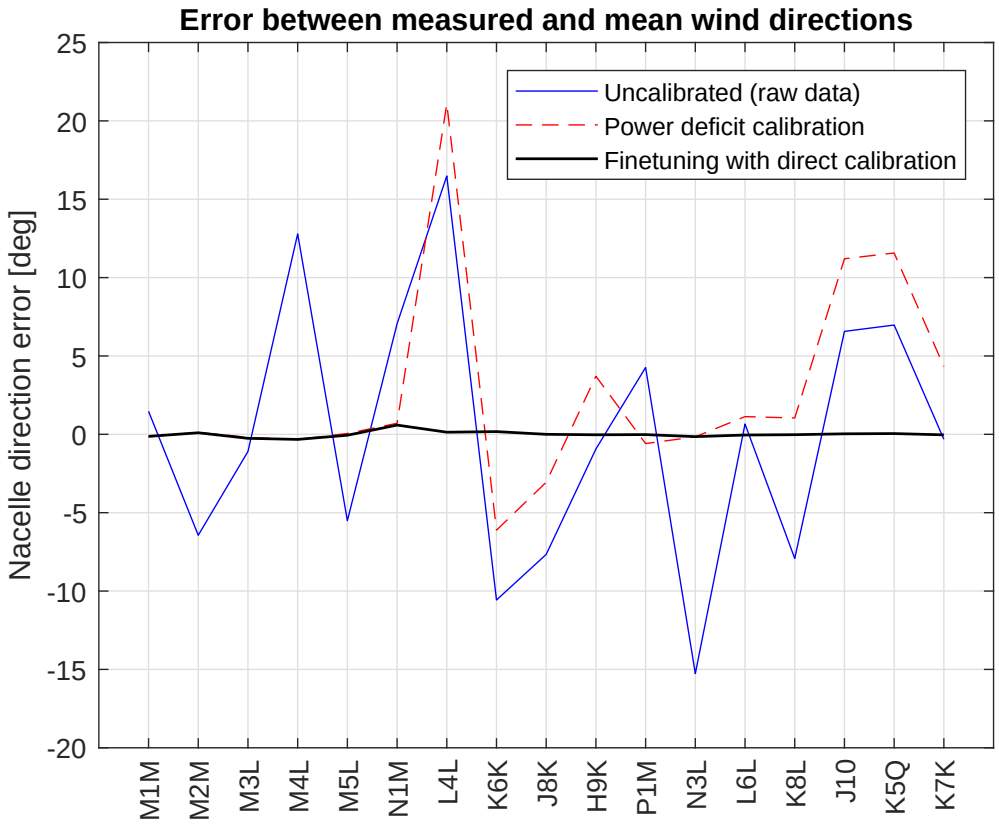

Figure 7: Mean error between individual nacelle direction measurements and the average of all turbines

As a result of above mentioned quality assurance criteria, some turbines will be left out from the power deficit based calibration process. These turbines are calibrated directly using the measurements from turbines that have been calibrated using the power deficit method. This is achieved using direct comparison of the measurement of a to-be-calibrated turbine to the measurements of the calibrated turbines. To account for the spatial variability of the wind, the weighted average of all calibrated measurements is used, with the weights being inversely proportional to the distance to the to-be-calibrated turbine.

The precise calibration method, used in this example, will be formalized below in more detail. Before doing that, let us first look at the calibration results for this example. Figure 6 gives the final calibrated nacelle direction measurements for the same period of one week as in Figure 4 (containing the original measurements). Clearly, measurement offsets in Figure 4 are absent in Figure 6, with the remaining differences between the signals being primarily stochastic in nature.

To assess the calibration accuracy, Figure 7 is provided. The figure depicts the mean error between the individual nacelle direction measurement and the circular average nacelle direction between all turbines. The blue line represents the original measurements, and exhibits large differences between the measurements at the individual turbines (as seen in Figure 4). The dashed red curve represents the error after the calibration using the power deficit method explained above. As explained above, the power deficit method is only applied to those turbines that pass the selected quality assurance criterion. For those turbines, the red dashed curve is close to zero, while for the remaining (uncalibrated) turbines significant deviations from the average are still present. After application of the direct calibration method to these remaining wind turbines, all large errors disappear (see the black solid line in Figure 7). The dif-

ferences between the calibrated measurements and the average wind direction are insignificant (the deviations of the black curve from zero are barely visible), all passing the accuracy quality test.

Table 1: Variation of the calibration offsets over periods of half year

	Calibration offset [°]				
Turbine ID	Period 1	Period 2	Period 3	Period 4	Max dev [°]
M1M	-5.76	-5.27	-5.03	-6.15	0.52
M2M	3.56	1.51	2.33	2.05	1.20
M3L	-2.48	-3.05	-3.43	-3.65	0.67
M4L	-15.81	-16.27	-17.17	-17.63	0.91
M5L	2.53	2.15	2.21	0.94	0.57
N1M	-10.18	-10.84	-11.61	-11.06	0.74
L4L	-19.66	-20.52	-19.84	-20.93	0.58
K6K	7.62	6.68	7.38	6.27	0.63
J8K	5.01	4.03	4.22	3.22	0.89
H9K	-4.18	-5.55	-4.74	-3.55	0.96
P1M	-7.32	-7.40	-9.23	-8.80	0.87
N3L	12.46	11.72	11.15	10.66	0.96
L6L	-3.76	-5.71	-4.75	-5.26	1.11
K8L	4.20	2.51	3.07	3.47	0.89
J10K	-9.09	-9.19	-9.71	-11.05	0.67
K5Q	-10.15	-11.88	-10.96	-11.41	0.95
K7K	-2.16	-2.78	-2.68	-4.17	0.79

Finally, the measurement data provided with a total duration of two years has been cut into four periods of half an year each, and the calibration method has been applied on each period. This was done to investigate if the calibration offsets vary with time. The calibration offsets of the turbines, computed for each separate half year period are listed in Table 1. The last column of the table provides the maximum deviation from the average over the four periods, which remains well below 1.5 degrees for all turbines. This calibration accuracy is very high and considered sufficient for the purpose of AWC validation.

The method for calibration of the nacelle direction measurements based on power deficit analysis, applied in Example 2 above, is next described in more detail for clarity. Let

$$\alpha^{(T_i)}(k) = \alpha_{nac}^{(T_i)}(k) + \alpha_{yaw}^{(T_i)}(k) \tag{4.4}$$

be the wind direction estimation at the i-th wind turbine T_i at time instant k, wherein $\alpha_{nac}^{(T_i)}(k)$ is the nacelle heading measurement, and $\alpha_{yaw}^{(T_i)}(k)$ is the yaw error measurement at the same turbine T_i. Let further $P^{(T_i)}(k)$ be the electric power measurement at T_i. The calibration of the nacelle direction measurement $\alpha_{nac}^{(T_i)}$ using the power deficit method requires

- power measurements $P^{(T_j)}(k)$, $j \in J^{(T_i)}$, collected at a set $J^{(T_i)}$ of neighbouring turbines for turbine i. The set $J^{(T_i)}$ contains:
  - The turbine T_i
  - The subset $J_{downstr}^{(T_i)}$ with turbines that are either in the direct wake of T_i, or in the direct wake of another turbine that is itself in the direct wake of T_i, for wind directions in which T_i is in free stream operation. Free stream operation is defined here as follows: T_i is in free stream for wind direction α if there are no turbines upstream of T_i within the wind direction sector

$(\alpha - 20°, \alpha + 20°)$. Direct wake is defined as follows: Turbine T_j is in direct wake of T_i if T_i is the closest upstream wind turbine that is waking T_j and the distance between T_i and T_j is not more than 20 rotor diameters.

  - The subset $J_{upstr}^{(T_i)}$ with upstream turbines of which T_i is in direct wake for some wind directions, but only if these are in free stream or in direct wake of a free stream turbine. Notice that a turbine can pertain to both $J_{downstr}^{(T_i)}$ and $J_{upstr}^{(T_i)}$, as T_i can be upstream of T_j for some wind directions and downstream for the opposite wind directions.

- power estimates $P_{model}^{(T_j)}(\alpha)$, $j \in J^{(T_i)}$, function of the ambient wind direction $\alpha \in A$, calculated for a single, partial load ambient wind velocity (e.g. 8 m/s) and for a representative set of wind directions $A \subset [0°, 360°)$ using a trusted wake model (such as FarmFlow [4]). A good practice is to take $A \subset \{0°, 1°, 2°, \ldots, 359°\}$.

Define the power measurements ratios $\delta P^{(i,j)}(k) = P^{(T_i)}(k) / P^{(T_j)}(k)$, and the estimated power ratios $\delta P_{model}^{(i,j)}(k, c) = P_{model}^{(T_i)}\left(\alpha^{(T_i)}(k) + c\right) / P_{model}^{(T_j)}\left(\alpha^{(T_i)}(k) + c\right)$ using the wake model. Here, the constant c serves as the to be computed calibration offset for turbine T_i. Notice that in the expression for $\delta P_{model}^{(i,j)}$ the wind direction $\alpha^{(T_i)}$ at turbine T_i only is used.

Next, define the time instances sets

$$K^{(i,j)} = \left\{k : 0 < P^{(T_i)}(k) < 0.95 P_r \cap 0 < P^{(T_j)}(k) < 0.95 P_r \cap \delta P^{(i,j)}(k) < \delta P_{max}\right\},$$

i.e. $K^{(i,j)}$ will contain time instances for which T_i and T_j are both in partial load operation (power production less than 95 % of rated power P_r), and the power ratio $\delta P^{(i,j)}$ is limited to δP_{max}. In Example 2 above this upper bound δP_{max} was chosen as 1.4, but it could also be set lower than that as long as it remains higher than one. It is not recommended to set it much higher than 1.4 as the calibration method here uses power deficit dips, not peaks.

The calibration offset $C^{(T_i)}$ for turbine T_i is then calculated as the solution to the following least squares problem

$$C^{(T_i)} = \arg\min_c f(c)$$

wherein the cost function $f(c)$ is defined as

$$\begin{aligned} f(c) \quad = \quad & \sum_{j \in J_{upstr}^{(i)}} \sum_{k \in K^{(i,j)}} \left(\delta P^{(i,j)}(k) - \delta P_{model}^{(i,j)}(k, c)\right)^2 \\ & + \sum_{j \in J_{downstr}^{(i)}} \sum_{k \in K^{(j,i)}} \left(\delta P^{(j,i)}(k) - \delta P_{model}^{(j,i)}(k, c)\right)^2 \end{aligned}$$

The calibrated nacelle direction measurement for turbine T_i is then

$$\alpha_{nac,clbr}^{(T_i)}(k) = \alpha_{nac}^{(T_i)}(k) + C^{(T_i)}. \tag{4.5}$$

Notice that in above optimization problem for the calibration offset $C^{(T_i)}$, the power ratios of T_i with all turbines T_j, $j \in J^{(T_i)}$, are included, where for the upstream turbines the ratio $P^{(T_j)}/P^{(T_i)}$ is used, while for the downstream ones the ratio used is $P^{(T_i)}/P^{(T_j)}$. This is to ensure that in both cases the power ratio dips are used in the optimization.

As discussed in Example 2, the calibration using the power deficit method, outlined above, applies only to turbines that pass the selected quality assurance criteria. Some of these, as those related to the limitation of the distance downstream and upstream, are already incorporated into the definitions of the subsets subset $J_{downstr}^{(T_i)}$ and $J_{upstr}^{(T_i)}$. In addition to these, for better conditioning of the power deficit method the terms $\delta P^{(i,j)}(k) - \delta P_{model}^{(i,j)}(k,c)$ in the cost function $f(c)$ could be excluded for all turbine pairs (i,j) for which $\delta P_{model}^{(i,j)}(k,c)$ has too many local minima. Finally, after the power deficit calibration process is completed for all turbines, an accuracy quality check needs to be applied to validate the accuracy of the calibration. The power deficit calibration is considered unsuccessful for those turbines that do not pass the accuracy quality test, being that the calibrated nacelle measurement should not deviate by more than 1° from the average nacelle direction value (the average is evaluated on the circle and using only the calibrated measurements).

For the turbines that are left out of the power deficit based calibration process, direct calibration can be performed using the measurements from turbines that are calibrated using the power deficit method. To this end, the average difference between the measurement of a to-be-calibrated turbine and the weighted sum of all calibrated measurements can be used. To account for the spatial variability of the wind, the weighted average of all calibrated measurements is used, with the weights being inversely proportional to the distance to the to-be-calibrated turbine.

Now that the calibration method for the nacelle heading measurements has been established, the focus is moved towards the construction of the WDTF. As explained at the beginning of this section, the WDTF constitutes the relationship between the wind direction measurement during intentional yaw misalignment and that during normal operation. As such, it is meant to provide a means to calibrate the biased yaw error measurements during intentional yaw misalignment.

Unfortunately, at the time of preparation of this document, no measurement data was available to properly exemplify the construction of the WDTF. For this purpose, operational data from two adjacent wind turbines in required: one operated with intentional yaw misalignment and the other one normally. In order to demonstrate at least the conceptual idea behind the WDTF, the measurement data from the single turbine operated with intentional yaw misalignment from Example 1 will be used in the next example.

Example 3 (Effect of misalignment on the yaw error measurement)

This example is based on the measurement data used in Example 1, collected from a turbine operating with intentional yaw misalignment with a range of yaw offset angle setpoints varying between −20° and 20°. The purpose of the example is to illustrate the effect of yaw misalignment on the yaw error measurement $\alpha_{yaw,iSpin}$ of the iSpin sensor. Since there is no data from adjacent wind turbines to serve as reference yaw measurement, the derived yaw error $\alpha_{yaw,clbr}$ will be used computed as the difference between the calibrated nacelle heading $(\alpha_{nac,iSpin} + C_{compass})$ measured by the iSpin, and the wind direction $\alpha_{wd,MM}$ measured at the nearby metmast. See Example 1 for details about the calibration of the iSpin nacelle heading measurement. In this example, only data from free stream operation of the test turbine is used, while operating in power production mode and the wind speed is below 12 m/s (partial load). Obvious outliers are removed as well.

The grey dots in Figure 8 represent the derived yaw error measurement $\alpha_{yaw,clbr}$ plot against the iSpin measurement of the yaw error $\alpha_{yaw,iSpin}$. These clearly deviate from the $y = x$ line (black dashed line). A least squares fit line (blue solid line) indicates the

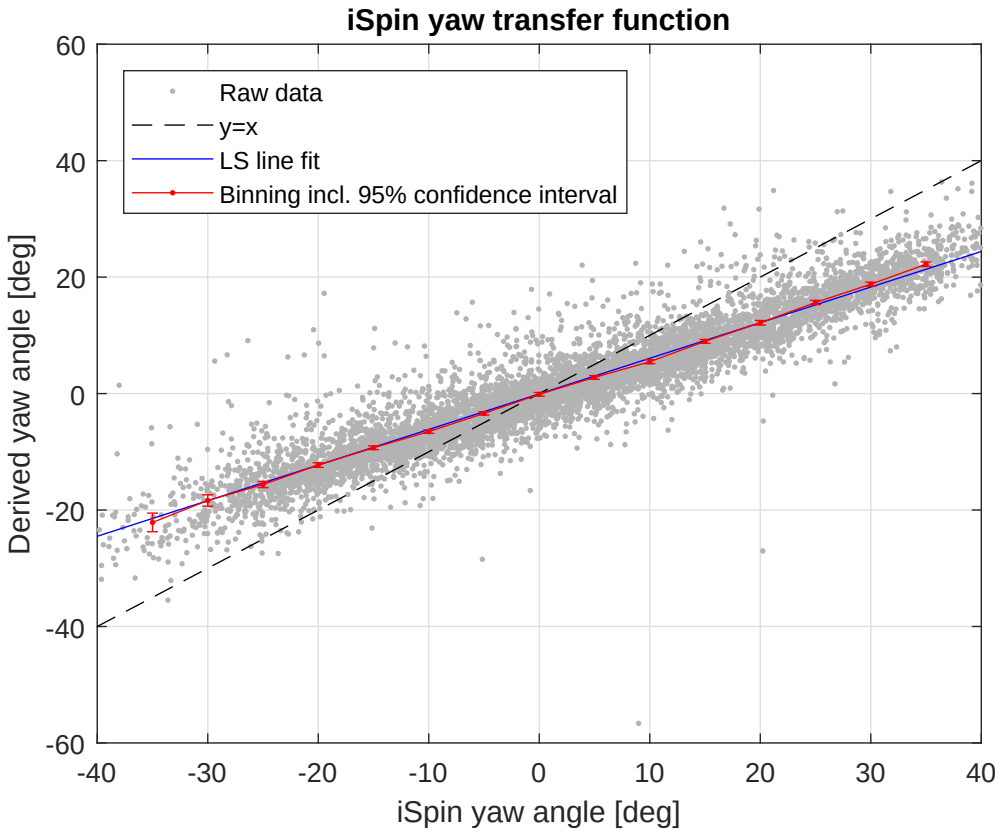

Figure 8: iSpin yaw error transfer function

presence of a quite significant slope difference, showing that the iSpin measurement exaggerates the actual yaw error. The red solid line in the figure, laying practically on top of the blue line, is constructed by binning the data at intervals of 5°. Although difficult to distinguish in the plot, the 95% confidence intervals are also plotted.

Finally, it should be mentioned that, although not shown in the figure, the wind velocity seems to have practically no effect on the line fit for these data. It can therefore be concluded that the linear least squares model, independent of the wind velocity, is a quite accurate representation of these data. Whether a similar conclusion also holds for the actual WDTF still needs to be investigated using appropriate measurement data.

The approach described above allows to derive calibrated wind direction measurements in which the effect of yaw misalignment is properly compensated. Using these, a single wind direction signal can be constructed which is representative for the whole wind farm. This signal will be called “consensus wind direction”, $\alpha_{WD,cons}$, and will be used in the process of binning, discussed in section 4.4. Similarly to the way the consensus wind speed, V_{cons}, was constructed in the previous section, $\alpha_{WD,cons}$ is computed as the average value of the corrected wind direction measurements at all wind turbine operating in free stream. Again, unavailable or non-operational wind turbines are excluded from the averaging. In order to determine which turbines are in free stream operation, the farm-average nacelle-based wind direction measurement can be used in combination with a simple wake expansion model, as explained in the previous section for the consensus wind speed.

4.3 Data filtering

To keep the uncertainty as low as possible and avoid getting biased results, it is essential that only good quality data are used in the analysis; the data should not be corrupted and should be obtained during normal operation. To ensure that, filtering is applied on the data. The following data filtering is recommended:

- *Power production*: for the AWC validation analysis, turbines need to be in power production mode. A suitable criterion to assure this is that the produced power is higher than some value, e.g. 1 % of the rated power. However, imposing this condition to all wind turbines in the farm can be too restrictive, especially for large wind farms. The reason for this is that, even when the individual turbine availability is high, the collective availability of all wind turbines at the same time is much lower. For instance, even when the turbine availability is as high as $P_{avail} = 97\,\%$, for a wind farm consisting of $N = 100$ turbines the probability that all turbines are available at the same time is $P^N_{avail} < 5\,\%$ (assuming that the turbine downtimes are independent). Therefore, filtering out all data records containing unavailable wind turbines will result in too little data records for proper statistical analysis. To avoid that, it is recommended to not reject data records containing some unavailable turbines, provided that there is at least some minimum number of normally operating turbines (e.g. 10 % of all) that are not affected by unavailable turbines through their (missing) wakes. This is important as unavailable turbines affect the power production downstream. To determine which turbines are affected by unavailable turbines upstream, a simple but conservative wake expansion model should be used, as explained in the section 4.1 for the consensus wind speed. How to properly process measurements containing missing entries from some of the turbines will be described in section 4.5.
- *Curtailment*: turbines that are only sporadically curtailed should be treated in the same way as unavailable turbines, i.e. excluding the measurements from curtailed turbines and turbines in their wakes from the analysis. Turbines that are always curtailed by some amount that remains consistent throughout the complete AWC validation campaign (i.e. curtailment amount is a fixed function of the undisturbed wind speed and/or wind direction, independent on the operating mode of the wind farm) may be treated in the same way as uncurtailed turbines.
- *Power boosting*: power boosting is treated in the same way as power curtailment.
- *Data quality*: it is recommended to exclude data from the analysis in the following circumstances:
  - failure or degradation of the measurement equipment (e.g. due to icing)
  - the standard deviation of the wind velocity measured at all operational free stream wind turbines is too large. The limit in this condition should be carefully chosen to avoid rejecting useful data.
  - the standard deviation of the wind direction measured at all operational free stream wind turbines is too large. The limit in this condition should be carefully chosen to avoid rejecting useful data.

4.4 Data binning

Binning will have to be applied not only to the wind speed, but also to the wind direction. This can easily result in a large number of bins with insufficient number of points within some bins, and therefore large uncertainty. For instance, considering narrow bins of 1 m/s for the wind velocity and 1° for the wind direction give rise to as many

as 7560 bins. Two months of 10-min data, uniformly distributed over all wind speeds and wind directions, and assuming full availability of all turbines, will result in just one data point per bin. As the tests are to be performed with two control modes (nominal and AWC), a complete test campaign duration of one year will result in two half-year data chunks or, on the average, around three data points per bin. Obviously, this is insufficient.

Due to the requirement to keep the duration of the AWC test campaign within one year, the above implies that the only feasible way to ensure sufficient number of measurements per bin is to make the bins larger. Increasing the bin size should be done with care though. Too large bins can deteriorate the accuracy of the AWC validation method since the variation of farm power production within a bin can be rather large. If, within a bin, the farm power production varies too much with the wind direction then the average power within that bin will depend significantly on the distribution of the measurements within that bin, which should be avoided. The same holds for power variations with the wind speed. Since the wind speed distribution (typically in the form of a Weibull distribution) usually varies a lot with the wind speed below rated, and since the power production varies a lot as well, it is not recommended to increase the size of the wind speed bins beyond 1 m/s.

Generally, it seems reasonable to choose the bin size such as to limit the uncertainty in the wind farm power production estimate to some specified limit. A good practice is to use the normalized standard error of the farm power per bin, defined as

$$\hat{\sigma}_{\bar{P}_b,norm} = \frac{\hat{\sigma}_{\bar{P}_{b,farm}}}{\bar{P}_{b,farm}}. \tag{4.6}$$

In the above expression, $\bar{P}_{b,farm}$ is the mean value of the wind farm power production $P_{b,farm}$ within bin b, and $\hat{\sigma}_{\bar{P}_{b,farm}}$ is the standard deviation of the mean $\bar{P}_{b,farm}$ (or, equivalently, the standard error of $P_{b,farm}$). By increasing the bin size, more data points will fall within the bin, causing $\hat{\sigma}_{\bar{P}_b,norm}$ to decrease. This allows to gradually increase the bin size until $\hat{\sigma}_{\bar{P}_b,norm}$ drops below a certain limit, $\hat{\sigma}^{max}_{\bar{P},norm}$. $\hat{\sigma}^{max}_{\bar{P},norm}$ can be hence seen as the highest acceptable normalized standard error for each bin (hard bound), but the bin size may further be increased in an attempt to get $\hat{\sigma}_{\bar{P}_b,norm}$ to drop further down towards a lower, desirable (soft) limit $\hat{\sigma}^{des}_{\bar{P},norm} < \hat{\sigma}^{max}_{\bar{P},norm}$. Notice that due to the non-uniform wind speed and direction distribution, this process will usually result in variable bin sizes over the range of wind conditions. This will be illustrated later on in Examples 4 and 5 in section 4.7.

To simplify the bin size choice process, one can best keep the bin size for the wind velocity fixed (1 m/s), and vary only the wind direction bin size, increasing it from 1° to some selected maximum wind direction bin size, b^{max}_{WD}. As mentioned above, the wind speed bin size should not be increased too much anyway as this would increase the standard deviation of the power measurements within the bin significantly. Moreover, keeping the wind speed bin size constant and small enough, and increasing the wind direction bin size instead to capture enough data, makes it possible to construct a power curve per wind direction bin. This has added value as it allows to study the impact of the AWC strategy on the power curve within each wind direction sector.

Now, let us focus on the computation of the statistical properties of the wind farm power production within a given bin. Suppose there are two sets of data, one containing data from the wind farm during nominal operation (without AWC), and another one with data gathered during periods with AWC active. Suppose further that the data from each of the two sets has been binned with respect to the consensus wind speed and consensus wind direction (described in sections 4.1 and 4.2). Let $P^{(s)}_{b,t,i}$ be the i-th power measurement ($i = 1, ..., N^{(s)}_b$) of t-th wind turbine ($t = \overline{1, N_t}$) within bin b

of data set s, $N_b^{(s)}$ be the total number of data records within bin b of data set s, and N_t be the number of turbines in the wind farm. Assuming, for the time being, that all measurements are available (no turbines are unavailable, curtailed or power boosted, and no data records are missing), and denoting the total power production of the wind farm within the i-th data record in bin b of data set s as

$$P_{b,i,farm}^{(s)} = \sum_{t=1}^{N_t} P_{b,t,i}^{(s)}. \tag{4.7}$$

the bin average power production value, standard deviation and standard error are given by the following equations, respectively

$$\bar{P}_{b,farm}^{(s)} = \frac{1}{N_b^{(s)}} \sum_{i=1}^{N_b^{(s)}} P_{b,i,farm}^{(s)}, \tag{4.8}$$

$$\hat{\sigma}^2\left(P_{b,farm}^{(s)}\right) = \frac{1}{N_b^{(s)}-1} \sum_{i=1}^{N_b^{(s)}} \left(P_{b,i,farm}^{(s)} - \bar{P}_{b,farm}^{(s)}\right)^2, \tag{4.9}$$

$$\hat{\sigma}^2\left(\bar{P}_{b,farm}^{(s)}\right) = \frac{1}{N_b^{(s)}} \hat{\sigma}^2\left(P_{b,farm}^{(s)}\right). \tag{4.10}$$

As pointed out above, these expressions would only work under the assumption that there is no missing data from any wind turbine in any data record i, i.e. $P_{b,t,i}^{(s)}$ are all available and usable. If within a given record i^* the measurement from even one single turbine t^* is missing (turbine unavailable), or not usable (turbine curtailed, power-boosted, or in wake of such turbine), the total wind farm power production $P_{b,i^*,farm}^{(s)}$ cannot be computed for that record i^*. Skipping all such records from the analysis is not desirable, as already explained in section 4.3, because it would result in skipping most of the data records, including lots of useful data from available wind turbines. In the next section, an alternative approach for computing the above bin-wise statistics that enables the use of data records including at least a minimum number of usable power measurements.

4.5 Turbine unavailability, curtailment and power-boosting

As discussed in section 4.4, the percentage of time that all turbines are available within a wind farm is very low, especially for wind farms with a large number of turbines. SCADA data can also show periods of unavailability even when turbines are in operation. Filtering out whole data records during periods of time with missing data from any of the turbines will leave only a very limited amount of data for analysis, and will necessitate too long a duration of the test campaign. To illustrate this, Figure 9 is provided. The figure depicts the power productions of all 111 wind turbines within Anholt offshore wind farm (see Example 4 later on for more information) for a randomly chosen bin, namely wind speed of 7.5 m/s to 8.5 m/s, and wind direction 269.5° to 270.5°. A total of 23 records of 10-min measurements is present in this bin from the measurement data of more than an year. The colored rectangles indicate the power production measurement on each turbine within each data record. White rectangles indicate missing data. A given measurement is labelled missing if either the turbine measurement is missing, or the turbine is not in normal mode of operation (i.e. it is unavailable, curtailed or power-boosted), or of is affected by the wake of such a turbine. In just 3 out of the 23 records all measurements are available for analysis, and rejecting all other 20 records will result in losing a very large amount of useful measurements.

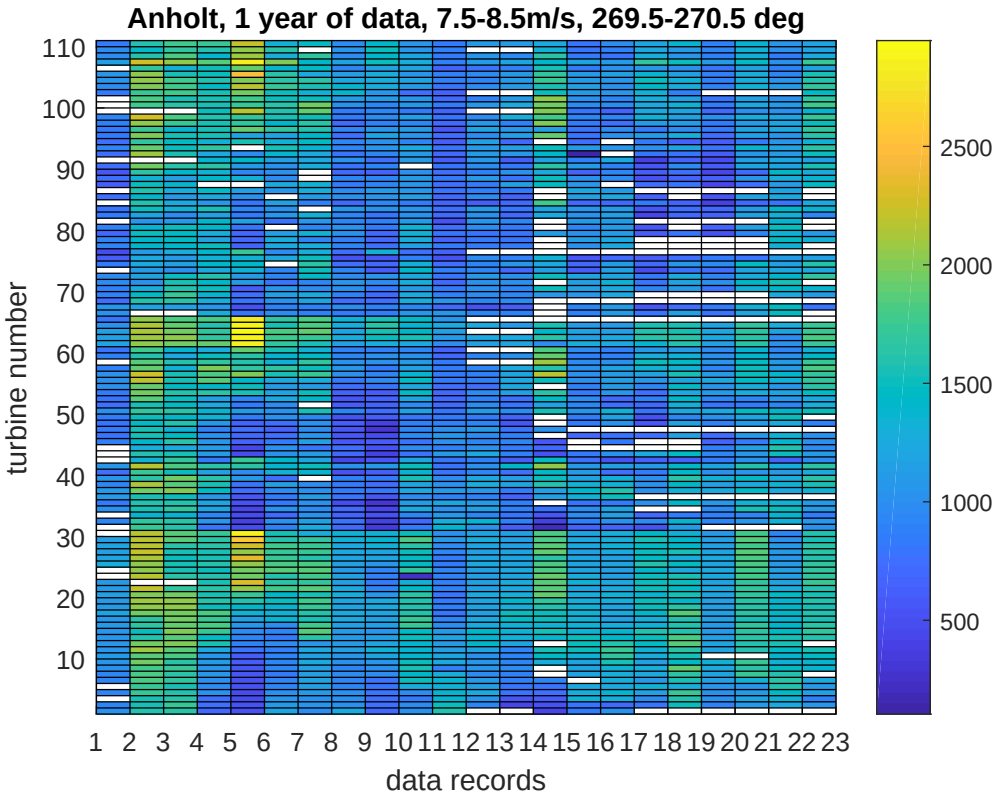

Figure 9: Power productions of all 111 wind turbines of Anhold wind farm from one year of measurements, that pertain to bin 7.5 m/s to 8.5 m/s and 269.5° to 270.5°. The white rectangles represent rejected data

To avoid this, a methodology is now proposed that allows to include data records into the analysis that contain some missing data. Instead of computing the wind farm power production for each record (as in equation (4.7)), the main idea is to first calculate the statistics for each individual turbines within the bin, and then derive the statistics for the wind farm power within the bin. More specifically, let $N_{b,t}^{(s)} \leq N_b^{(s)}$ be the number of non-missing power measurements for turbine t within bin b of data set s. Then the following relations describe the t-th turbine statistics within bin b of data set s:

$$\bar{P}_{b,t}^{(s)} = \frac{1}{N_{b,t}^{(s)}} \sum_{i=1}^{N_{b,t}^{(s)}} P_{b,t,i}^{(s)}, \tag{4.11}$$

$$\hat{\sigma}^2\left(P_{b,t}^{(s)}\right) = \frac{1}{N_{b,t}^{(s)}-1} \sum_{i=1}^{N_{b,t}^{(s)}} \left(P_{b,t,i}^{(s)} - \bar{P}_{b,t}^{(s)}\right)^2, \tag{4.12}$$

$$\hat{\sigma}^2\left(\bar{P}_{b,t}^{(s)}\right) = \frac{1}{N_{b,t}^{(s)}} \hat{\sigma}^2\left(P_{b,t}^{(s)}\right). \tag{4.13}$$

For the average power production it then holds

$$\bar{P}_{b,farm}^{(s)} = \sum_{t=1}^{N_t} \bar{P}_{b,t}^{(s)}. \tag{4.14}$$

It can easily be shown that when there is no missing data within the bin (i.e. $N_{b,t}^{(s)} = N_b^{(s)}$ for all turbines), then this expression for $\bar{P}_{b,farm}^{(s)}$ is equivalent to that in equation

(4.7) in section 4.4. To calculate the standard deviation $\hat{\sigma}(P^{(s)}_{b,farm})$ and standard error $\hat{\sigma}(\bar{P}^{(s)}_{b,farm})$ of $P^{(s)}_{b,farm}$, the following expressions can be used, which are a direct consequence of applying the general relations for propagation of error in measurements described in [5]

$$\hat{\sigma}^2\left(P^{(s)}_{b,farm}\right) = \sum_{t_1=1}^{N_t}\left(\hat{\sigma}^2\left(P^{(s)}_{b,t_1}\right) + \sum_{t_2=1}^{N_t}\hat{\sigma}^2\left(P^{(s)}_{b,t_1}, P^{(s)}_{b,t_2}\right)\right), \tag{4.15}$$

$$\hat{\sigma}^2\left(\bar{P}^{(s)}_{b,farm}\right) = \sum_{t_1=1}^{N_t}\left(\hat{\sigma}^2\left(\bar{P}^{(s)}_{b,t_1}\right) + \sum_{t_2=1}^{N_t}\hat{\sigma}^2\left(\bar{P}^{(s)}_{b,t_1}, \bar{P}^{(s)}_{b,t_2}\right)\right), \tag{4.16}$$

wherein the the cross-variances are defined, similarly to the auto-variances in Equations (4.12)-(4.13), as follows

$$\hat{\sigma}^2\left(P^{(s)}_{b,t_1}, P^{(s)}_{b,t_2}\right) = \frac{1}{N^{(s)}_{b,t_1,t_2}-1}\sum_{i=1}^{N^{(s)}_{b,t_1,t_2}}\left(P^{(s)}_{b,t_1,i} - \bar{P}^{(s)}_{b,t_1}\right)\left(P^{(s)}_{b,t_2,i} - \bar{P}^{(s)}_{b,t_2}\right), \tag{4.17}$$

$$\hat{\sigma}^2\left(\bar{P}^{(s)}_{b,t_1}, \bar{P}^{(s)}_{b,t_2}\right) = \frac{1}{N^{(s)}_{b,t_1,t_2}}\hat{\sigma}^2\left(\bar{P}^{(s)}_{b,t_1}, \bar{P}^{(s)}_{b,t_2}\right). \tag{4.18}$$

In the above expressions, $N^{(s)}_{b,t_1,t_2} \leq \min\{N^{(s)}_{b,t_1}, N^{(s)}_{b,t_2}\}$ is the number of records containing non-missing pairs of power measurements for turbines (t_1, t_2) within bin b of data set s.

4.6 Atmospheric conditions

For a single wind turbine, the power performance measurements standard IEC 61400-12-1:2017 [1] describes the normalizations that should be applied to air density, turbulence intensity and wind shear. These are meant to enable the comparison of results from different data sets bringing them to a similar scale. This standard suggests that these normalizations have the purpose to improve the accuracy of the results.

The wind shear correction requires that the wind velocity is measured at different heights, so that the effect of wind shear on the power measurement can be accounted for. However, one of the requirements on the AWC validation methodology, stated in section 2, stipulates that only the on-site available measurement equipment may be used (basically only the SCADA data). This implies that one cannot assume the availability of (free stream) wind speed measurements at different heights. Therefore, wind shear corrections will not be applied in the analysis.

The air density can be determined by measuring the ambient air temperature, air pressure and relative humidity (i.e. not internal nacelle conditions, neither measurements behind the rotor, cf. [2, §7.4]). As such measurements are not considered conventionally available, air density normalization will also be excluded from the analysis.

The turbulence intensity of the free stream is also not available for all wind directions in many sites. Although it might be possible to determine a way to derive a method for (rough) estimation of the turbulence intensity of the free stream by using the nacelle based (behind the rotor) wind speed measurements, this is considered pointless. There are two reasons for that. Firstly, the turbulence intensity estimate will contain a significant level of uncertainty which would, to a large extend, destroy the intended accuracy improvement aimed by including turbulence intensity normalization into the analysis. Secondly, most of the turbines often operate in a wake situation, where the turbulence levels are much higher than those in free stream and even more uncertain.

Therefore, including turbulence intensity normalization is not considered as a viable way to increase the accuracy of the AWC validation method.

In summary, no measurements of the atmospheric conditions will be used in the AWC validation methodology.

4.7 Power ratio calculation

In section 4.5 expressions were provided for the computation of the mean value, standard deviation and standard error of the wind farm power production within a given wind bin. These expressions, given by equations (4.14)-(4.16), and applicable even when data records contain missing data from some of the turbines, will form the basis for the computation of the statistics for the power ratio. These are derived in this section, both for a given wind bin and for the weighted average.

For a given wind bin b, the ratio between the wind farm power productions from two different data sets (called power ratio in the sequel) is defined as

$$\delta P_b = \frac{P^{(1)}_{b,farm}}{P^{(2)}_{b,farm}} \tag{4.19}$$

For the mean value, standard deviation and standard error of δP_b, the following expressions are a direct consequence of application of the relations provided in [5]

$$\widehat{\delta P}_b = \frac{\bar{P}^{(1)}_{b,farm}}{\bar{P}^{(2)}_{b,farm}} \tag{4.20}$$

$$\begin{aligned}
\hat{\sigma}^2_{\delta P_b} &= \left(\frac{\partial \widehat{\delta P}_b}{\partial \bar{P}^{(1)}_{b,farm}}\right)^2 \hat{\sigma}^2\left(P^{(1)}_{b,farm}\right) + \left(\frac{\partial \widehat{\delta P}_b}{\partial \bar{P}^{(2)}_{b,farm}}\right)^2 \hat{\sigma}^2\left(P^{(2)}_{b,farm}\right) \\
&= \left(\frac{1}{\bar{P}^{(2)}_{b,farm}}\right)^2 \hat{\sigma}^2\left(P^{(1)}_{b,farm}\right) + \left(\frac{\bar{P}^{(1)}_{b,farm}}{\left(\bar{P}^{(2)}_{b,farm}\right)^2}\right)^2 \hat{\sigma}^2\left(P^{(2)}_{b,farm}\right) \\
&= \frac{1}{\left(\bar{P}^{(2)}_{b,farm}\right)^2}\left(\hat{\sigma}^2\left(P^{(1)}_{b,farm}\right) + \left(\widehat{\delta P}_b\right)^2 \hat{\sigma}^2\left(P^{(2)}_{b,farm}\right)\right)
\end{aligned} \tag{4.21}$$

$$\hat{\sigma}^2_{\widehat{\delta P}_b} = \frac{1}{\left(\bar{P}^{(2)}_{b,farm}\right)^2}\left(\hat{\sigma}^2\left(\bar{P}^{(1)}_{b,farm}\right) + \left(\widehat{\delta P}_b\right)^2 \hat{\sigma}^2\left(\bar{P}^{(2)}_{b,farm}\right)\right) \tag{4.22}$$

In order to calculate the weighted average power production, the frequency distribution per wind bin is required. Clearly, the same frequency distribution must be used for both data sets as otherwise there will be differences in the weighted average power productions due to differences in the frequency distribution rather than due to AWC operation. There are two ways to obtain the wind bin frequency distribution: either using provided site-specific (joint) wind speed and direction probability density function, or by using the actual number of records within each bin to directly construct the frequency distribution using the measurement data from the AWC validation campaign. Using the one or the other, for each wind bin a weight $0 \leq \alpha_b \leq 1$, $b = \overline{1, B}$, is determined such that $\sum_{b=1}^{B} \alpha_b = 1$, B being the number of bins. The weight α_b will represent the probability that the wind conditions fall within wind bin b, and should be representative for both data sets.

When the weighted average power ratio analysis is to be performed using a provided site-specific joint wind speed and direction probability density function $f(V, \alpha_{WD})$, with

V and α_{WD} being the wind speed and wind direction, respectively, the weights are determined as follows

$$\tilde{\alpha}_b = \int_{V_b^{min}}^{V_b^{max}} \int_{\alpha_{WD,b}^{min}}^{\alpha_{WD,b}^{max}} f(V, \alpha_{WD}) d\alpha_{WD} dV, \tag{4.23}$$

$$\alpha_b = \frac{\tilde{\alpha}_b}{\sum_{b=1}^{B} \tilde{\alpha}_b}. \tag{4.24}$$

In the expression above, V_b^{min}, V_b^{max}, $\alpha_{WD,b}^{min}$ and $\alpha_{WD,b}^{max}$ denote the lower and upper bounds for the wind speed and wind direction within bin b.

The alternative way of computing the wind bin weightings is by using the actual number of records within each bin, $N_b^{(s)}$. This can be achieved using the following expression, which ensures that the weights will be the same for both data sets

$$\alpha_b = \frac{N_b^{(1)} + N_b^{(2)}}{\sum_{b=1}^{B} \left(N_b^{(1)} + N_b^{(2)} \right)}. \tag{4.25}$$

Given the wind bin weighting factors α_b, the weighted average power ratio is defined as

$$\delta P_{av} = \frac{P_{av}^{(1)}}{P_{av}^{(2)}} = \frac{\sum_{b=1}^{B} \alpha_b P_{b,farm}^{(1)}}{\sum_{b=1}^{B} \alpha_b P_{b,farm}^{(2)}} \tag{4.26}$$

It should be pointed out here that, whenever the weightings α_b have been determined using a joint probability density function, or using actual measurements from AWC validation campaign with a duration of one year (or multiples of that), the weighted wind farm power productions $P_{av}^{(s)}$ will represent the annual averages, and δP_{av} will then be the annual power ratio.

The following expressions, which can easily be derived using the results in [5], provide estimates of the mean value, standard deviation and standard error of δP_{av}

$$\widehat{\delta P}_{av} = \frac{\bar{P}_{av}^{(1)}}{\bar{P}_{av}^{(2)}} = \frac{\sum_{b=1}^{B} \alpha_b \bar{P}_{b,farm}^{(1)}}{\sum_{b=1}^{B} \alpha_b \bar{P}_{b,farm}^{(2)}} \tag{4.27}$$

$$\begin{aligned}
\hat{\sigma}^2_{\delta P_{av}} &= \sum_{b=1}^{B} \left(\frac{\partial \widehat{\delta P}_{av}}{\partial \bar{P}_{b,farm}^{(1)}} \right)^2 \hat{\sigma}^2 \left(P_{b,farm}^{(1)} \right) + \left(\frac{\partial \widehat{\delta P}_{av}}{\partial \bar{P}_{b,farm}^{(2)}} \right)^2 \hat{\sigma}^2 \left(P_{b,farm}^{(2)} \right) \\
&= \sum_{b=1}^{B} \frac{\alpha_b^2}{\left(\bar{P}_{av}^{(2)} \right)^2} \hat{\sigma}^2 \left(P_{b,farm}^{(1)} \right) + \left(-\alpha_b \frac{\bar{P}_{av}^{(1)}}{\left(\bar{P}_{av}^{(2)} \right)^2} \right)^2 \hat{\sigma}^2 \left(P_{b,farm}^{(2)} \right) \\
&= \frac{1}{\left(\bar{P}_{av}^{(2)} \right)^2} \sum_{b=1}^{B} \alpha_b^2 \hat{\sigma}^2 \left(P_{b,farm}^{(1)} \right) + \left(\widehat{\delta P}_{av} \right)^2 \alpha_b^2 \hat{\sigma}^2 \left(P_{b,farm}^{(2)} \right)
\end{aligned} \tag{4.28}$$

$$\hat{\sigma}^2_{\widehat{\delta P}_{av}} = \frac{1}{\left(\bar{P}_{av}^{(2)} \right)^2} \sum_{b=1}^{B} \alpha_b^2 \hat{\sigma}^2 \left(\bar{P}_{b,farm}^{(1)} \right) + \left(\widehat{\delta P}_{av} \right)^2 \alpha_b^2 \hat{\sigma}^2 \left(\bar{P}_{b,farm}^{(2)} \right) \tag{4.29}$$

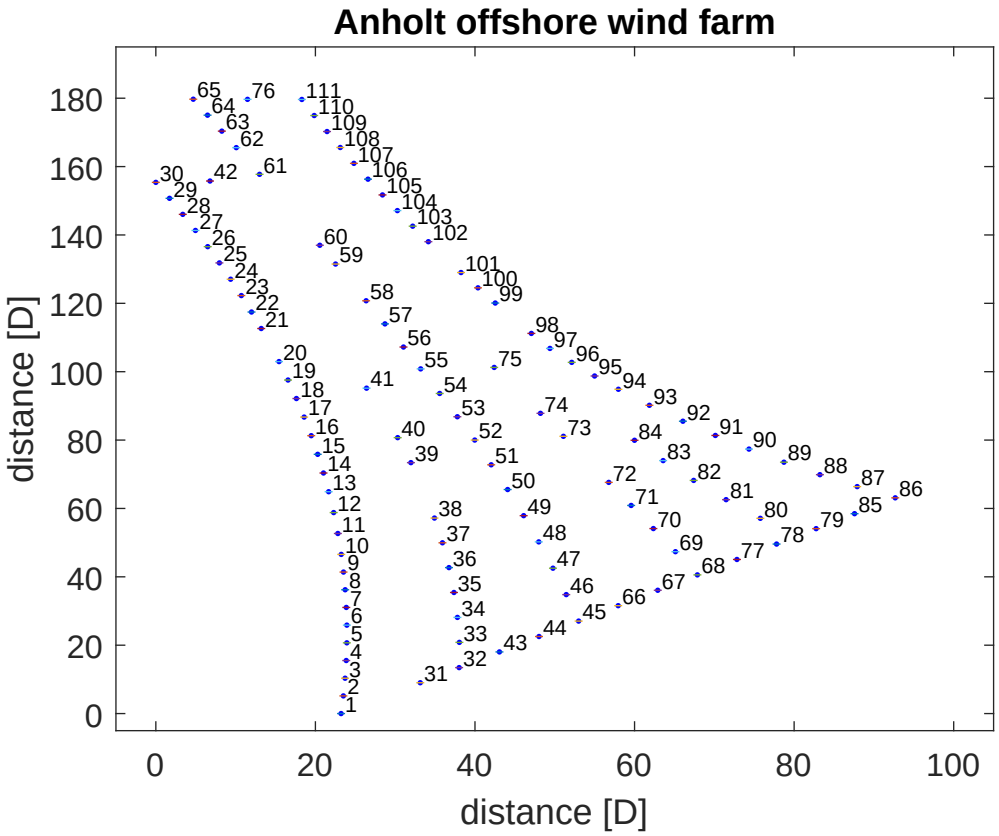

Figure 10: Layout of Anholt offshore wind farm

The process for deriving the power ratio will next be illustrated in two numerical examples. The examples are based on 2,5 years of SCADA data from the offshore wind farms Westermost Rough and Anholt, provided by Ørsted. All measurements are obtained during operation of the wind farms without AWC. To illustrate the analysis, the measurement data will be divided, for each wind farm, into two data sets. The analysis should ideally result in a power ratio equal to one, both for each bin ($\widehat{\delta P}_b$) and in terms of weighted average ($\widehat{\delta P}_{av}$). Both cases are very challenging as there is a large amount of missing data from unavailable wind turbines.

Example 4 (Power ratio analysis for offshore wind farm Anholt) *This example illustrates the power ratio analysis, presented above, on 2,5 years of SCADA data from offshore wind farm Anholt, operated by Ørsted. The farm is located approximately 21 km off the Danish shore, and consists of 111 Siemens wind turbines of the type SWT-3.6-120 (rated power of 3.6 MW, and rotor diameter of 120 m). The layout is depicted in Figure 10. The wind farm has a total capacity of 400 MW. The SCADA data shared by Ørsted includes 10-min statistics (mean, standard deviation, min and max values) for a number of signals, including the active power, wind velocity, nacelle direction, blade pitch angle, rotational speed, and others (used, for instance, for identifying curtailment or power boost periods).*

The measurement data has been processed as follows:

1. *Calibration of the nacelle direction measurements to remove constant biases: this is done following the approach discussed in section 4.2. A WDTF is not determined afterwards as the measurements do not include operation with yaw misalignment (nominal operation only).*

2. *Determination of consensus wind speed and wind direction: this is done as outlined at the end of sections 4.1 and 4.2.*

3. *Formation of two data sets: since the data is collected all during nominal operation without AWC, the available data is divided into two sets. This is done in a way to imitate the effect of toggling between reference and AWC operation. To this end, the data is divided into intervals of 2 hours, the uneven intervals are clustered into the first data set, and the even intervals form the second data set.*

4. *Data filtering: performed as outlined in section 4.3. Data records in which power measurement data is missing from more than 12 wind turbines is excluded from the analysis. Besides the unavailable measurements, measurements from turbines that are curtailed, power boosted, or such that are in the wake of unavilable/curtailed/power-boosted turbines, are also treated as missing when filtering the data. Also excluded are records that do not pass the data quality criteria, namely that the standard deviation of the wind speed and (calibrated) nacelle direction measurements of the wind turbines are larger than 2.5 m/s and 10°, respectively. This is to avoid that there are too large differences between the individual turbine measurements. The total amount of data records that passed the filtering process was around 50% for each of the two data sets, which boils down to around 9 months of data in each data set.*

5. *Data binning: done according to the approach outlined in section 4.4. The bin size for the wind velocity is kept constant equal to 1 m/s. The bin size for the wind direction is varying to ensure that the normalized standard error of the wind farm power is below* $\hat{\sigma}^{max}_{\bar{P},norm} = 0.05$*, as close as possible to the (soft) limit* $\hat{\sigma}^{des}_{\bar{P},norm} = 0.02$*. A maximum wind direction bin size of* $b^{max}_{WD} = 12°$ *is selected. The bin size selection process converged to the wind direction sectors illustrated in Figure 11. The figure depicts the normalized standard error of the wind farm power for initially selected fine bin size of 1 m/s by 1° for both data sets (green and yellow lines), and for the finally selected bin sizes (blue line). The levels indicated by the blue line represent the worst of the normalized standard errors of the wind farm power for the two data sets, which clearly lie within the selected hard and soft limits (dashed lines). Notice that wind direction sectors have variable sizes, and that there are wind directions that do not lie in any sector. This is due to the frequency distribution for the wind direction: some directions are much less frequent and need to be clustered into larger sectors to ensure that the normalized standard error gets within the limits. Whenever no sector size of length no longer that* b^{max}_{WD} *can be found that satisfies the limits mentioned above, the corresponding wind directions are skipped from the analysis. This can be observed in Figure 11 for wind directions around 150° and just below 360°, where no sectors have been formed.*

6. *Power ratio analysis*

    - *Power curves: the calculation of the power curves is performed in accordance with the expressions in equations* (4.14)-(4.16)*. Here, as an example, Figures 12 and 13 are provided. The figures illustrate the power curves for two selected wind direction sectors: one around 180°, i.e. for wind directions along the length of the farm (Figure 12); and one around 270°, i.e. for winds along the width of the farm (Figure 13). The figures give the mean wind farm power productions for the two data sets along with the 95 % confidence intervals (calculated as* $\pm 1.96 \hat{\sigma}_{\widehat{\delta \bar{P}}_b}$ *for bin* b*, i.e. assuming normal distribution). Clearly, the power curves compare very well, suggesting no difference in the power performance between the two data sets.*
    - *Power ratio per wind direction sector: the mean power ratio per wind direction sector is depicted by the thick red lines in Figure 14. The mean values are calculated over the wind speeds up to 11 m/s, to ensure that the power*

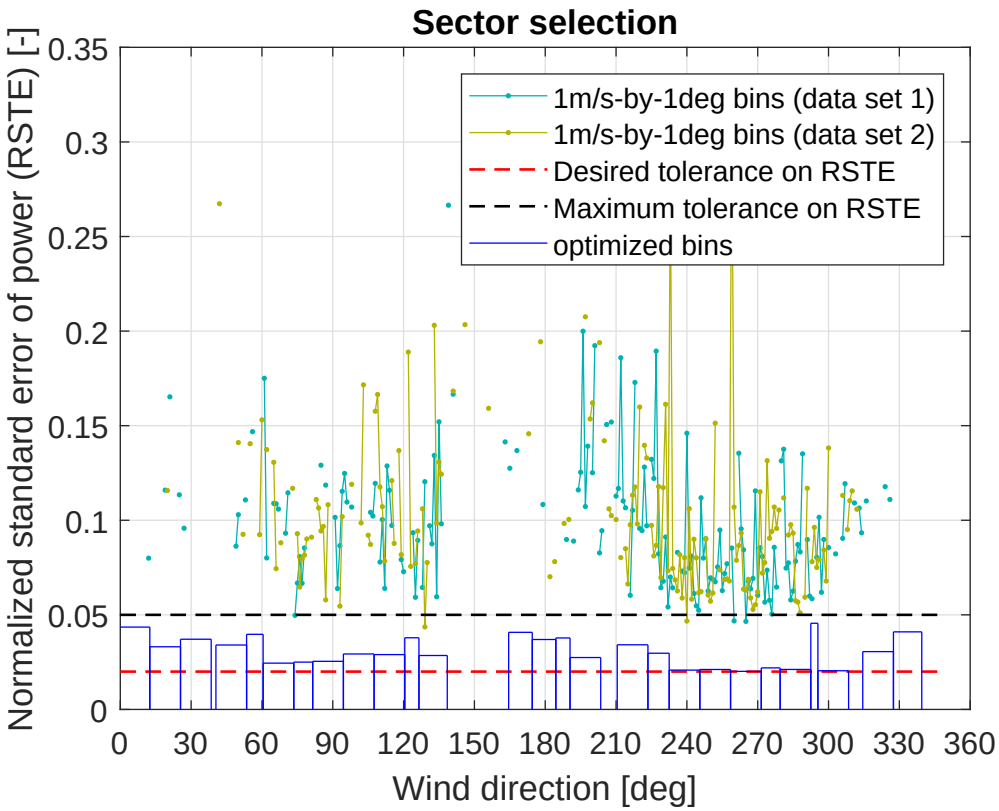

Figure 11: Wind direction sector size selection for Anholt wind farm

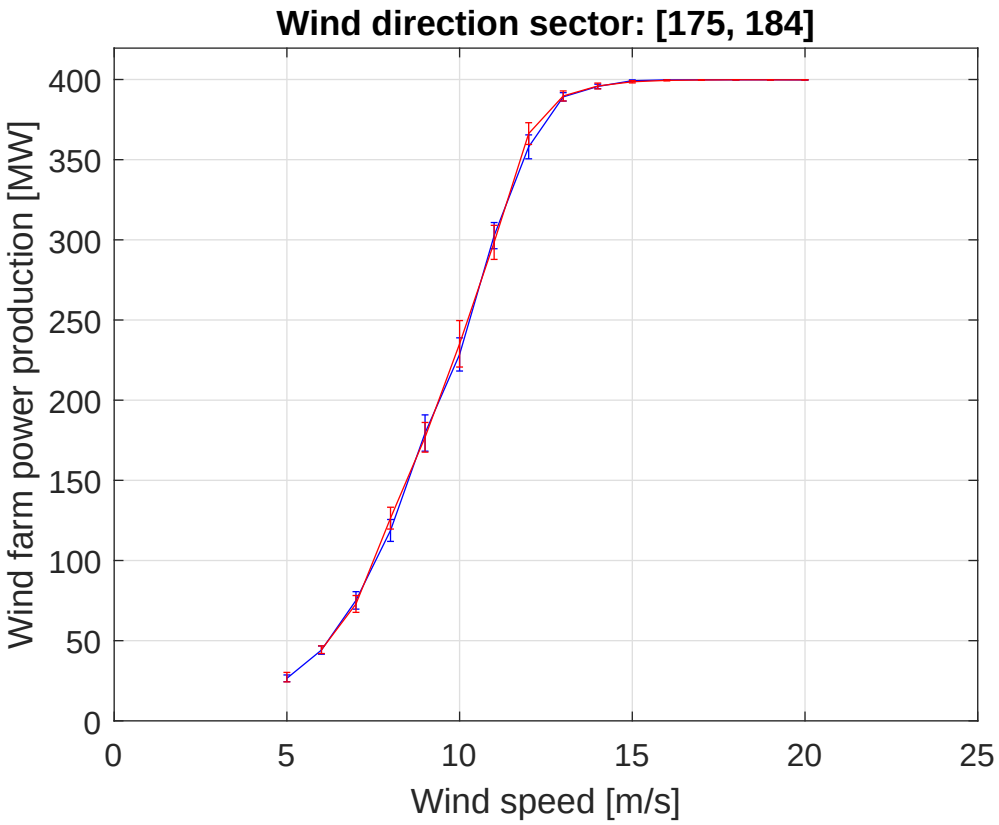

Figure 12: Power curves for Anholt wind farm, wind direction sector 175° to 184°: data set 1 (blue) and 2 (red)

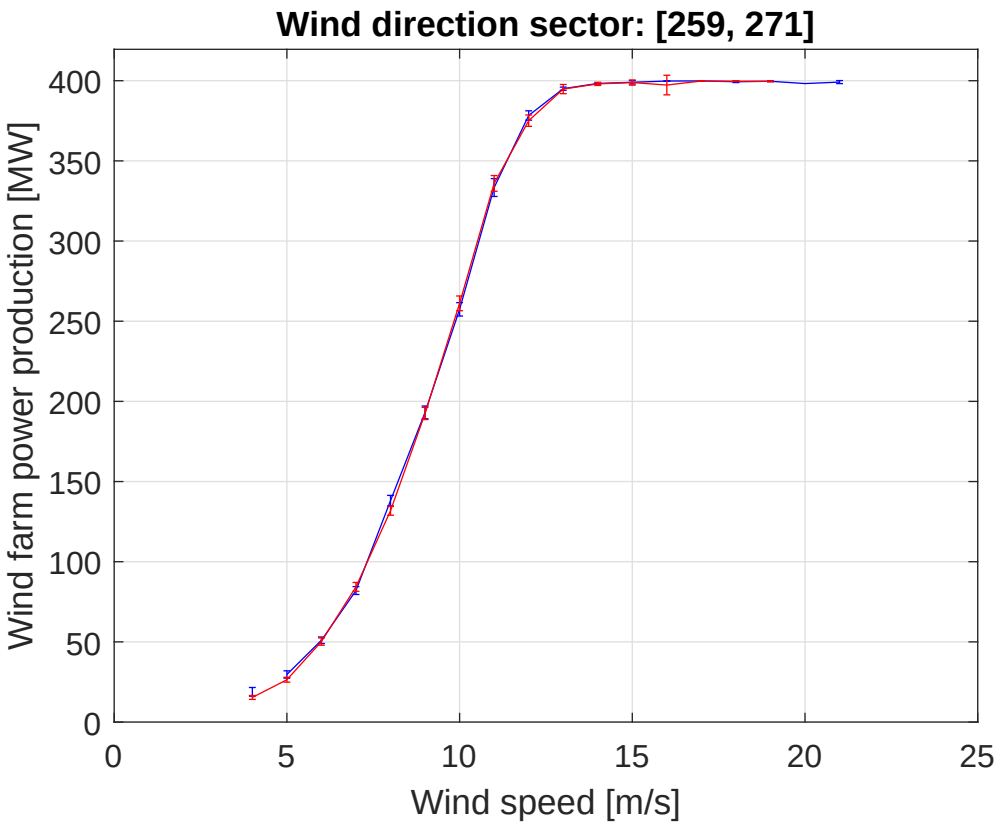

Figure 13: Power curves for Anholt wind farm, wind direction sector 259° to 271°: data set 1 (blue) and 2 (red)

ratio analysis, that is primarily of interest for the below rated wind region, does not get biased by above rated operation of the wind farm. The corresponding 95 % confidence levels are illustrated in the figure by the grey bars. It can be observed from the figure that for most sectors the mean power ratio lies within just 2 % from the expected value of 1, with an uncertainty of about ± 3.5 *% or less. This is considered as a rather accurate result, good enough to assess the potential power gain from AWC, which is expected to be significantly higher.*

- *Weighted average power ratio: using the relationships in equations* (4.27)-(4.29)*, the mean value of the weighted average wind farm power production,* $\widehat{\delta P}_{av}$*, has been calculated as 1.0006 with 95 % confidence interval of* $\pm 0.001\,66$ *around the mean value.*

Example 5 (Power ratio analysis for offshore wind farm Westermost Rough) *This example illustrates the power ratio analysis, presented above, on 2,5 years of SCADA data from offshore wind farm Westermost Rough, operated by Ørsted. The farm is located in the North sea approximately 8km off the English shore, and consists of 35 Siemens wind turbines of the type SWT-6.0-154 (rated power of 6 MW, and rotor diameter of 154 m). The layout is depicted in Figure 15. The wind farm has a total capacity of 210 MW. The SCADA data shared by Ørsted includes 10-min statistics (mean, standard deviation, min and max values) for a number of signals, including the active power, wind velocity, nacelle direction, blade pitch angle, rotational speed, and others (used, for instance, for identifying curtailment or power boost periods).*

The measurement data has been processed in the same way as in Example 4 above

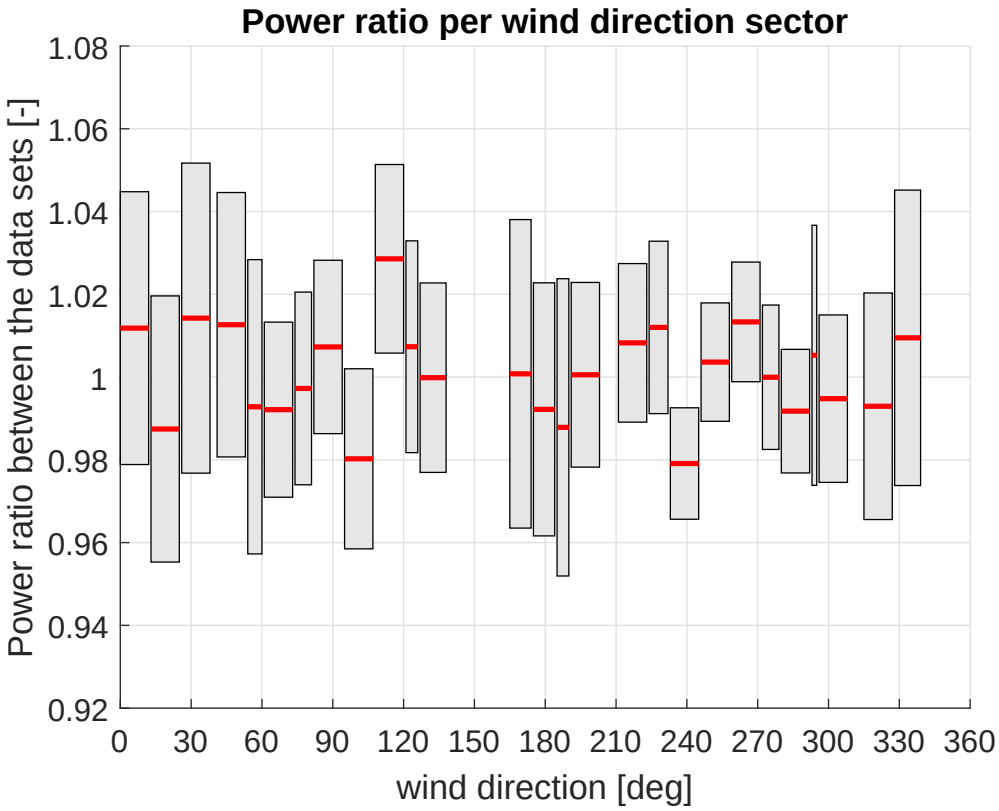

Figure 14: Power ratio per wind direction sector for the Anholt wind farm: mean value (red) and 95 % confidence interval (gray bars)

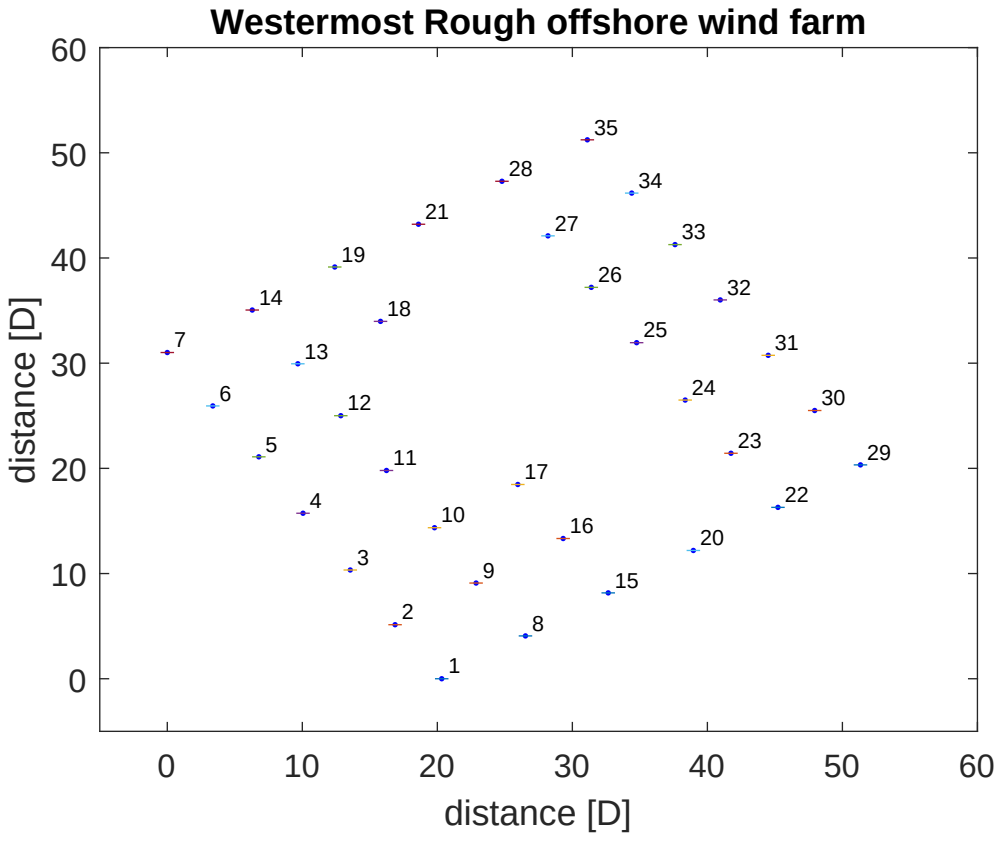

Figure 15: Layout of Westermost Rough offshore wind farm

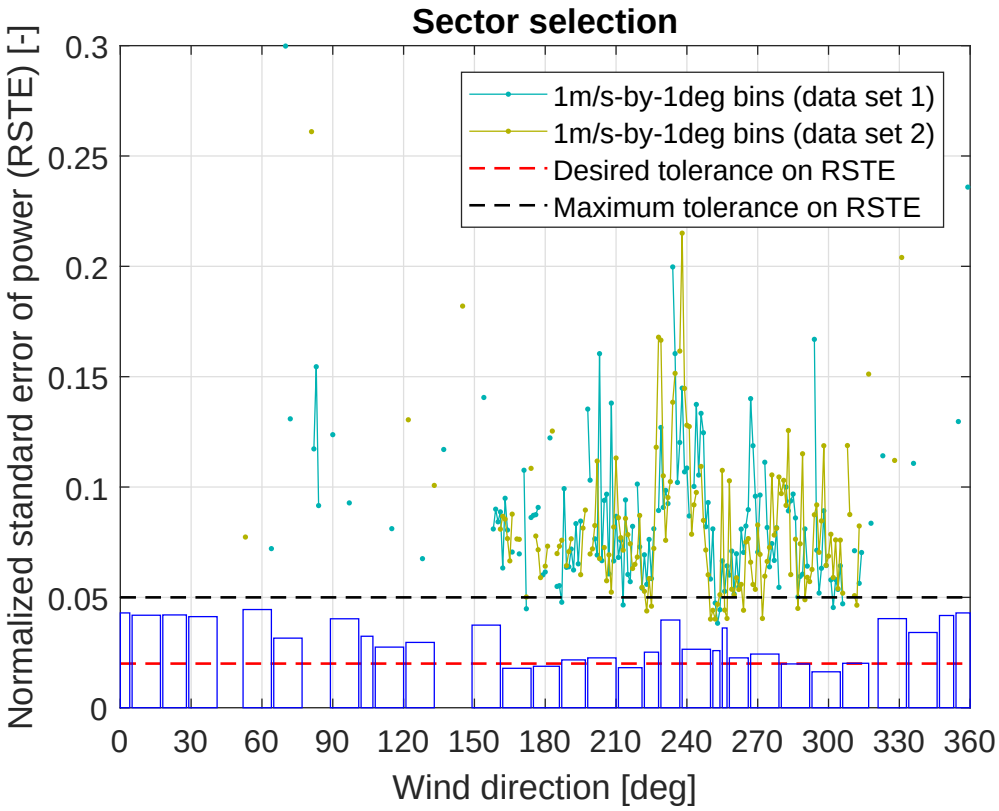

Figure 16: Wind direction sector size selection for Westermost Rough wind farm

and, hence, here the discussion of the results in mainly focused on the differences.

1. *Calibration of the nacelle direction measurements to remove constant biases: as in Example 4.*
2. *Determination of consensus wind speed and wind direction: as in Example 4.*
3. *Formation of two data sets: as in Example 4.*
4. *Data filtering: as in Example 4. Data records in which power measurement data is missing from more than 4 wind turbines is excluded from the analysis. The total amount of data records that passed the filtering process was around 36 % for each of the two data sets, which boils down to around 6.5 months of data in each data set.*
5. *Data binning: as in Example 4. The selected wind direction sectors are given in Figure 16, which is similar to Figure 11 in Example 4.*
6. *Power ratio analysis*
   - *Power curves: the power curves for two selected wind direction sectors are provided: one around 180° (Figure 17), and one around 270° (Figure 18). These power curves compare well.*
   - *Power ratio per wind direction sector: the mean power ratio per wind direction sector (thick red lines), together with the 95 % confidence levels (grey bars), are given by the thick red lines in Figure 19. For most sectors, the mean power ratio lies within 2.5 % from the expected value of 1, with an uncertainty of about ± 3.5 % or less is most cases. This result is considered enough to enable the assessment the potential power gain from AWC.*

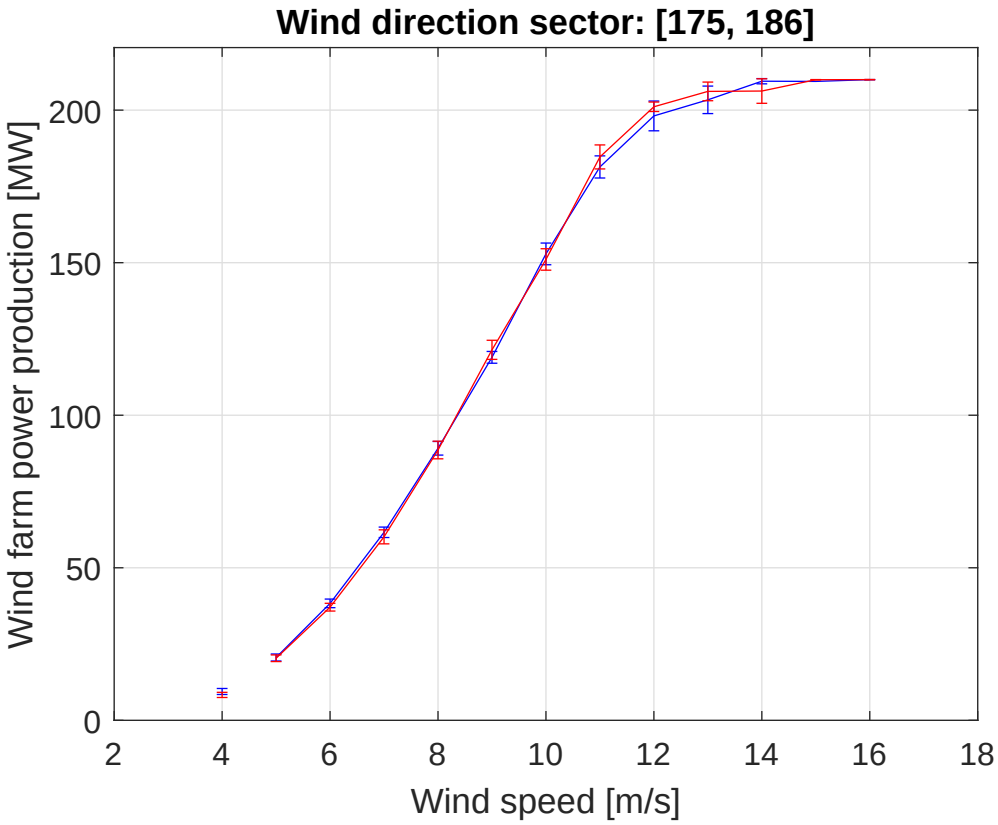

Figure 17: Power curves for Westermost Rough wind farm, wind direction sector 175° to 186°: data set 1 (blue) and 2 (red)

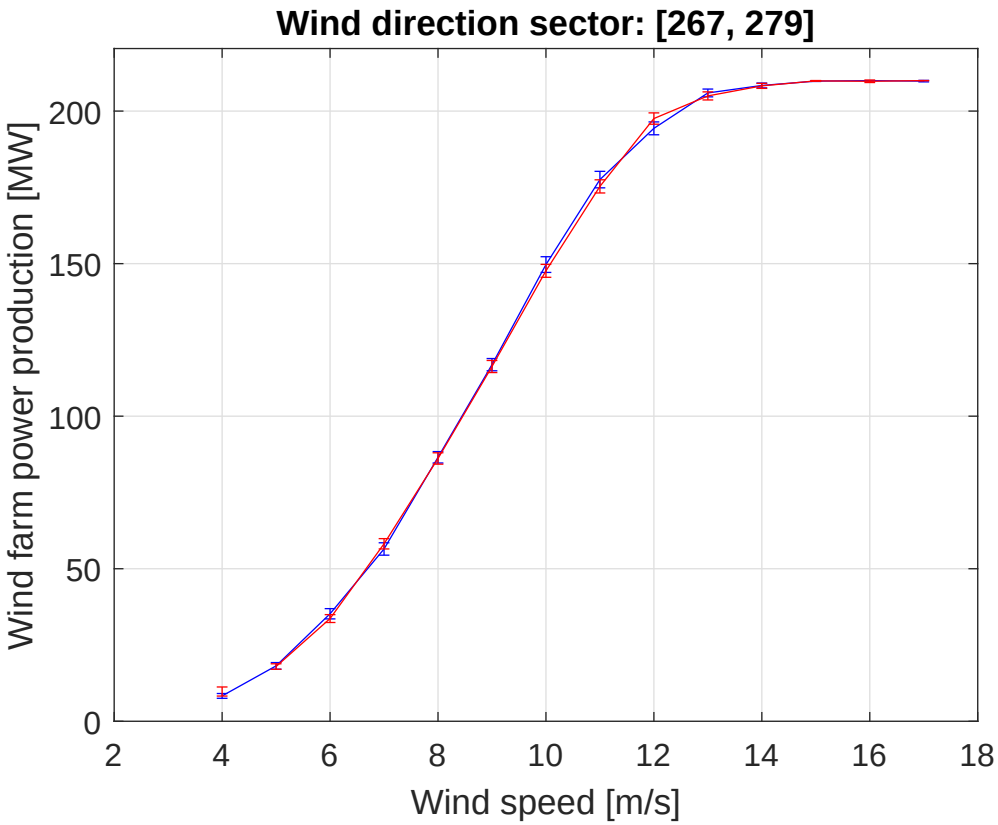

Figure 18: Power curves for Westermost Rough wind farm, wind direction sector 267° to 279°: data set 1 (blue) and 2 (red)

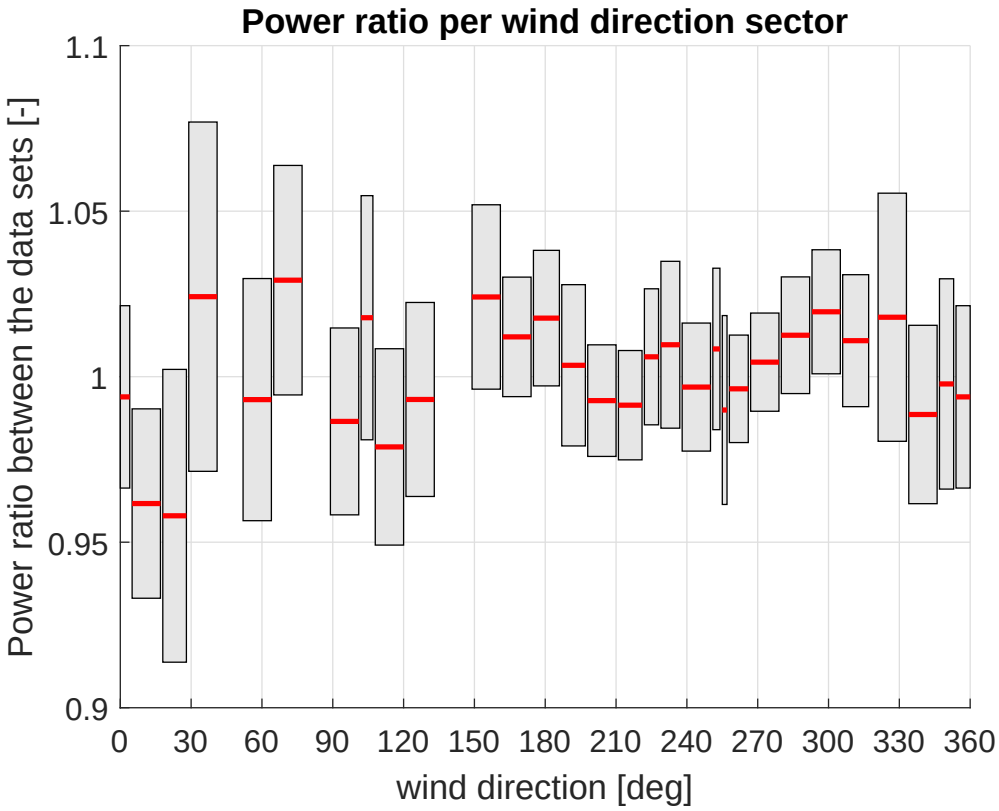

Figure 19: Power ratio per wind direction sector for the Westermost Rough wind farm: mean value (red) and 95 % confidence interval (gray bars)

- *Weighted average power ratio: the mean value of the weighted average wind farm power production, $\widehat{\delta P}_{av}$, has been calculated as 1.0016 with 95 % confidence interval of* ± 0.0024 *around the mean value.*

4.8 Impact of the toggle period

As explained earlier, the generic layout requirement essentially excludes the possibility for side-by-side testing. Therefore, the wind farm operation must be toggled between nominal operation without AWC, and operation with AWC. It is expected that the shorter the toggle period the more comparable the wind conditions within the two data sets are. Too short switching intervals, however, are not desirable as they would require more frequent activation and deactivation of the operation under yaw misalignment and, therefore, increased yaw activity. Something more: due to the slow yaw dynamics there will be a significant time lost in the rotors moving from operation under yaw misalignment to nominal (aligned) operation and visa versa. These transients will result in a larger portion of the data being skipped from the analysis than when the toggle interval is longer. This motivates the need to study the effect of the toggle period on the quality of the final power ratio estimate, which is the purpose of this section.

This is done by means of the following example.

Example 6 (Impact of the toggle period on the power ratio analysis) *The purpose of this example is to study the impact of the toggle period on the mean power ratio and its uncertainty, expressed in terms of the 95 % confidence interval. To this end, the SCADA data from offshore wind farms Anholt and Westermost Rough will be used, discussed in Examples 4 and 5, respectively. The data has also been processed in*

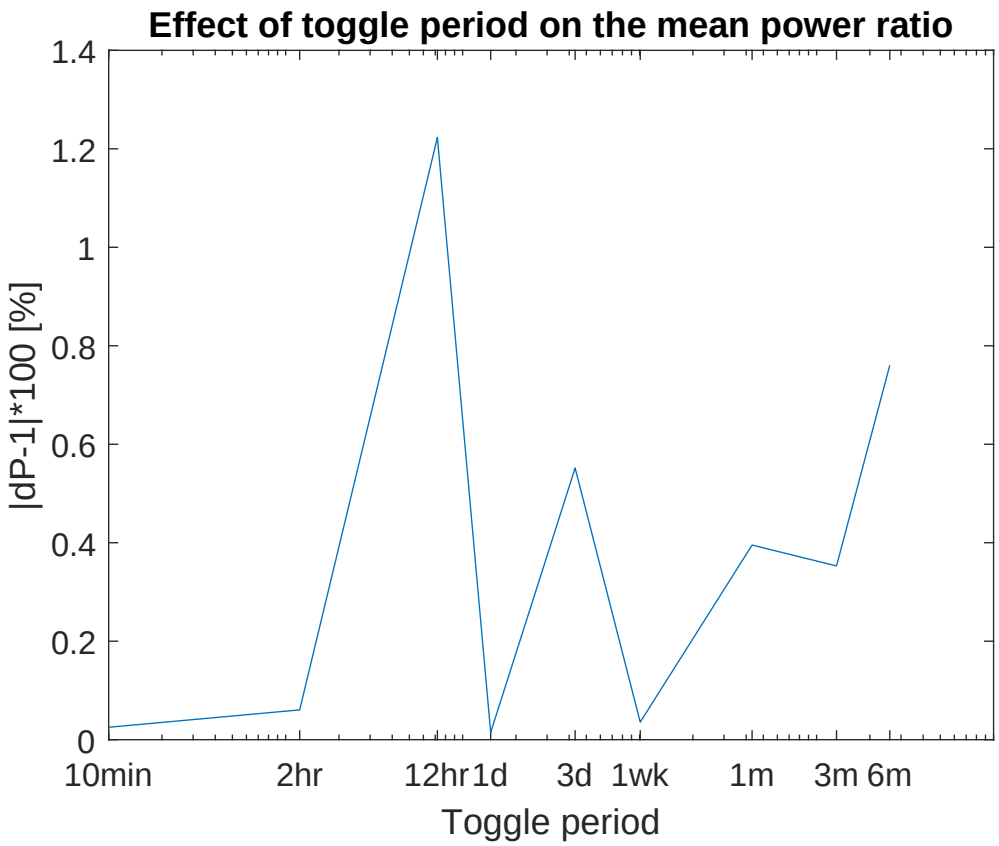

Figure 20: Effect of the toggle period on the mean power ratio for Anholt wind farm

exactly the same manner as outlined in mentioned examples, with the only difference that the toggle period has been varied between 10 minutes and 6 months to evaluate its impact on the results from the analysis.

Figures 20 and 21 depict the variation of the mean power ratio with the toggle period for the two wind farms. On the y-axis, the absolute variation of the mean farm power around the value of one is given in percentage, i.e. $100.|\widehat{\delta P}_{av} - 1|$ *[%]. It can be observed in both figures that the mean power ratio features a large peak at toggle period of 12 hours. This can be explained with the diurnal cycle: the two data sets then each contain only samples from one half of the diurnal cycle. For this specific example, at toggle period of 12 hours results in data set 1 containing only data between midnight and noon, and data set 2 - data between noon and midnight. This is expected to result in the data sets featuring different atmospheric stability, resulting in larger variation in the mean power ratio.*

Figures 22 and 23 show the variation of the uncertainty in the mean power ratio estimate, expressed as the 95 % confidence interval normalized to the mean power ratio in percentage, i.e. $100(1.96\hat{\sigma}_{\widehat{\delta P}_{av}}/\widehat{\delta P}_{av})$ *[%]. It can be seen that the uncertainty generally increases with the toggle period, but only very gradually. The most pronounced increase occurs between 2 hours and 12 hours.*

Based on the results, presented in Example 6, the following conclusions can be made:

- toggle period of 12 hours should be avoided as it significantly decrease the accuracy of the mean power ratio estimate. This is due to the fact that toggling

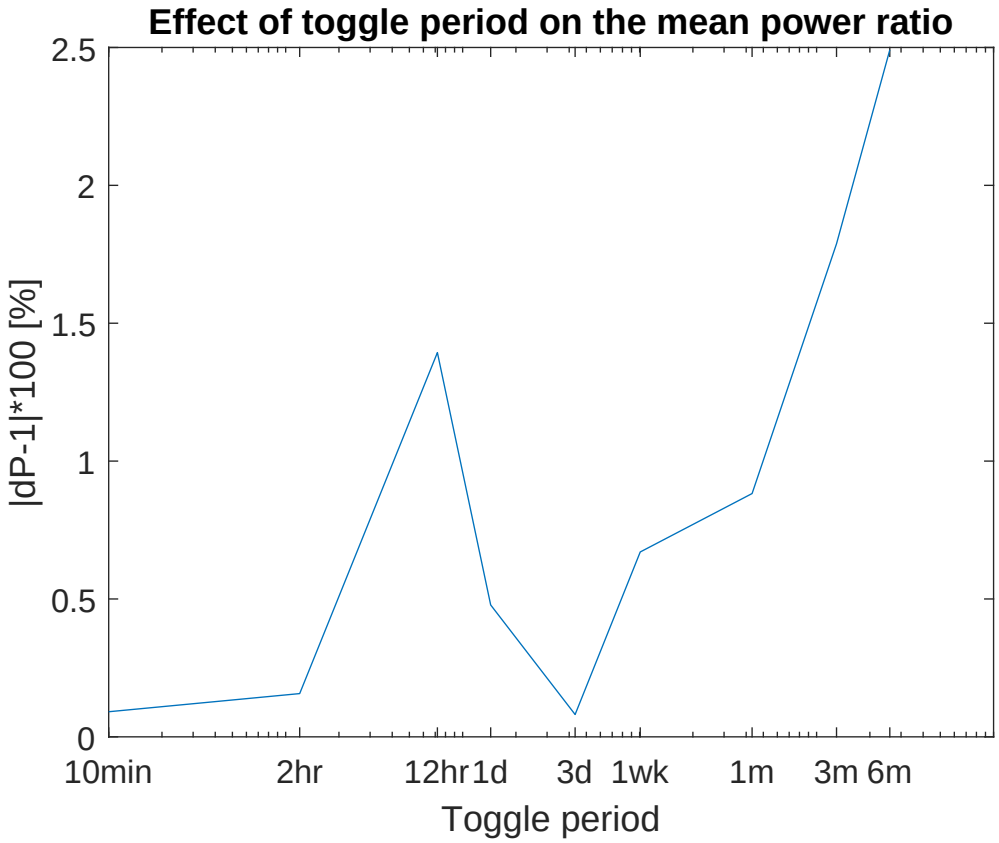

Figure 21: Effect of the toggle period on the mean power ratio for Westermost Rough wind farm

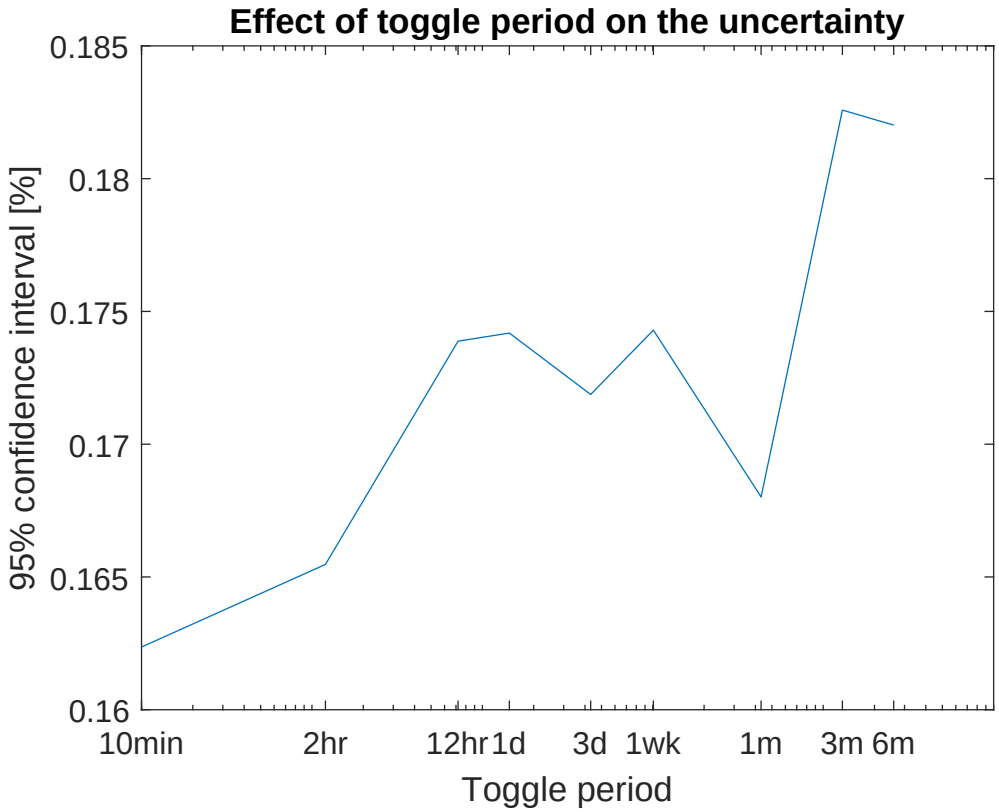

Figure 22: Effect of the toggle period on the 95 % confidence interval for the mean power ratio for Anholt wind farm

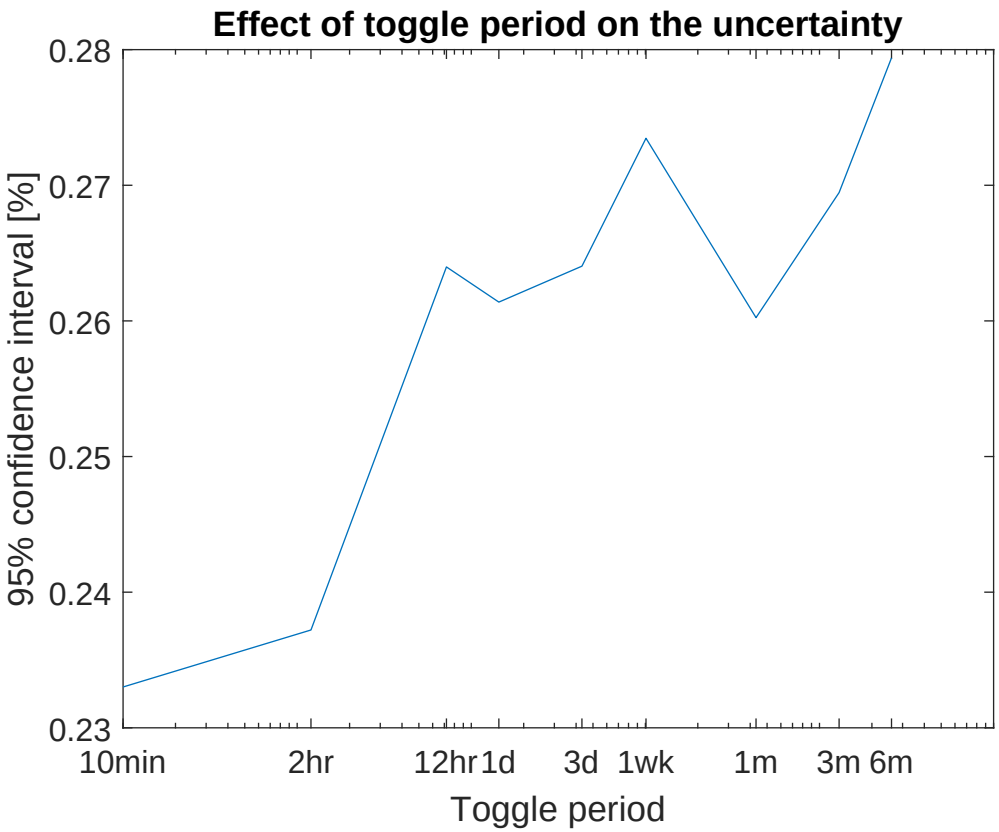

Figure 23: Effect of the toggle period on the 95 % confidence interval for the mean power ratio for Westermost Rough wind farm

at half the diurnal cycle may result in the two data sets featuring consistently different atmospheric conditions.

- best results, both in terms of mean power ratio and its uncertainty, are obtained for toggle periods of 2 hours or less.
- increasing the toggle period has a very weak, though negative, impact on the uncertainty.

Based on these conclusions, the general recommendation for the choice of the toggle period is

- 2-3 hours if the resulting yaw duty is not an issue, or otherwise
- 1 day to 1 week, but as short as possible.

4.9 Uncertainty quantification

The uncertainty analysis, proposed in this section, is aligned with the approach of the IEC 61400-12-2:2013 standard [2], Annexes E, F, H and I. There, the A and B category uncertainty components are first developed separately for the NTF and the nacelle power curve. Here the same lines of reasoning are followed: first the uncertainty components related to the process of determination of the WSTF and WDTF are listed, then those affecting the calculation of the consensus wind speed and wind direction, and finally those for the wind farm power production and power ratio. In doing that, an attempt is made to use as much as possible the uncertainty components' definitions and their notation from IEC 61400-12-2:2013. We will therefore not

go into detailed discussion here on each source of uncertainty but will focus on the differences with the IEC 61400-12-2:2013 standard; the reader is referred to [2] for more information.

The uncertainty components identified for the AWC validation methodology are listed in Tables 2, 3, 4, 5, and 6. These tables are discussed separately below. Common for all of them are their columns, listing:

- (first column) the uncertainty component,
- (second column) the corresponding category: A and B category uncertainties are considered, according to the definition in [2],
- (third column) the sensitivity coefficient,
- (fourth column) the mathematical notation used for the component,
- (fifth column) the magnitude used within the case studies in this section, which are here only meant to exemplify the uncertainty assessment method. Most of these values have been adopted from the examples in Annex G in [2],
- (sixth column) a note related to the source of the uncertainty component, e.g. about whether the component is already existing in IEC 61400-12-2:2013 or newly added here for the AWC validation methodology, or about the choice for its magnitude or sensitivity parameter value. The legend at the bottom of the table describes the notation used in this column.

Uncertainty in the WSTF measurement

As described in section 4.1, the WSTF is constructed using measurements from two adjacent wind turbines standing in free stream wind, one operating normally and the other – with intentional yaw misalignment. The measurements required to construct the WSTF are the nacelle wind speed at both turbines and the yaw error at the misaligned turbine. These can be identified in Table 2 as three of the main uncertainty components for the WSTF. The first one (nacelle wind speed measurement at the unyawed turbine), including its subcomponents and their magnitudes, is directly adopted from IEC 61400-12-2:2013. For the components related to the measurements at the yawed turbine, the subcomponents are chosen equivalently to these for the unyawed turbine. Same holds for their magnitudes. Besides the uncertainty components related to the measurement equipment, there are two other components in Table 2, related to the impact of seasonal variations onto the WSTF, and the variance in the measured WSTF (the only A category uncertainty). The sensitivity of the WSTF to the nacelle yaw error at the yawed turbine (chosen 0.05 in the table) has been determined using the Sedini measurement data from Example 1. The magnitude of (some of) the uncertainty components in Table 2 depend on the wind speed within a given bin (V_i), and do not depend on the wind direction as the WSTF is measured in free stream wind conditions.

Assuming full contribution of each uncertainty component, the combined uncertainty in the WSTF for wind speed bin V_i can then be written as

$$u_{WSTF,i} = \sqrt{u_N^2 + u_{YNi}^2 + u_{YWDEi}^2 + u_{MWSTFi}^2 + s_{WSTFi}^2} \tag{4.30}$$

Table 2: Uncertainty components for the WSTF

Uncertainty component	Cat.	Sens.	Notation	Magnitude	Note
Nacelle wind speed at unyawed turbine		c_{Ni}	u_{Ni}	**[m/s]**	
Calibration uncertainty due to wind speed	B	1	u_{N1i}	0.15	a
Calibration uncertainty due to wind direction	B	1	u_{N2i}	$0.01V_i$	a
Operational characteristics	B	1	u_{N3i}	$0.12 + 0.012V_i$	a
Mounting effects	B	1	u_{N4i}	$0.02V_i$	a
Data acquisition system	B	1	u_{dNi}	0.03	a
Nacelle wind speed at yawed turbine		c_{YNi}	u_{YNi}		
Calibration uncertainty due to wind speed	B	1	u_{YN1i}	0.15	b,c
Calibration uncertainty due to wind direction	B	1	u_{YN2i}	$0.01V_i$	b,c
Operational characteristics	B	1	u_{YN3i}	$0.12 + 0.012V_i$	b,c
Mounting effects	B	1	u_{YN4i}	$0.02V_i$	b,c
Data acquisition system	B	1	u_{dYNi}	0.03	b,c
Nacelle yaw error at yawed turbine		c_{YWDEi}	u_{YWDEi}		f
Calibration sensor mounting position	B	0.05	u_{YWD3i}	1	b,c
Calibration maximum bin averaged wind direction difference due to wind direction	B	0.05	u_{YWD4i}	2	b,c
Calibration maximum bin averaged wind direction difference due to non-vertical flow	B	0.05	u_{YWD5i}	2	b,c
Sensor alignment	B	0.05	u_{YWD6i}	2	b,c
Rotor effect on measured yaw error	B	0.05	u_{YWD7i}	0	b,c
Data acquisition system	B	0.05	u_{dYWD2i}	0.1	b,c
Method					
Seasonal variation on WSTF	B	1	u_{MWSTFi}	$0.02V_i$	b,d
Transfer function					
Variance in WSTF	A	1	s_{WSTFi}	$0.11 + 0.02V_i$	b,e
Notes					
a: as in IEC61400-12-2:2013, Annex F&G					
b: newly defined component					
c: Same value chosen as for corresponding component for unyawed turbine					
d: Same value chosen as for nacelle transfer function in IEC61400-12-2:2013					
e: estimated using measurement data from Sedini wind farm					
f: value for sensitivity coefficient estimated using measurement data					

wherein the combined uncertainties of the separate main components are given by the expressions

$$u_{Ni} = \sqrt{c_{Ni}^2 \left(\sum_{k=1}^{4} u_{Nki}^2 \right) + c_{Ni}^2 u_{dNi}^2}$$

$$u_{YNi} = \sqrt{c_{YNi}^2 \left(\sum_{k=1}^{4} u_{YNki}^2 \right) + c_{YNi}^2 u_{dYNi}^2}$$

$$u_{YWDEi} = \sqrt{c_{YWDEi}^2 \left(\sum_{k=3}^{7} u_{YWDki}^2 \right) + c_{YWDEi}^2 u_{dYWD2i}^2}$$

Table 3: Uncertainty components for the WDTF

Uncertainty component	Cat.	Sens.	Notation	Magnitude	Note
Nacelle yaw position at unyawed turbine		c_{WDPi}	u_{WDPi}	deg	
Calibration	B	1	u_{WD1i}	2.5	a,h
Signal resolution	B	1	u_{WD2i}	0.5	a
Data acquisition	B	1	u_{dWD1i}	0.1	a
Nacelle yaw position at yawed turbine		c_{YWDPi}	u_{YWDPi}		
Calibration	B	1	u_{YWD1i}	2.5	b,c
Signal resolution	B	1	u_{YWD2i}	0.5	b,c
Data acquisition	B	1	u_{dYWD1}	0.1	b,c
Nacelle yaw error at unyawed turbine		c_{WDEi}	u_{WDEi}		
Calibration sensor mounting position uncertainty	B	1	u_{WD3i}	1	a
Calibration maximum bin averaged wind direction difference due to wind direction	B	1	u_{WD4i}	2	a
Calibration maximum bin averaged wind direction difference due to non-vertical flow	B	1	u_{WD5i}	2	a
Sensor alignment	B	1	u_{WD6i}	2	a
Rotor effect on measured yaw error	B	1	u_{WD7i}	0	a
Data acquisition system	B	1	u_{dWD2i}	0.1	a
Nacelle yaw error at yawed turbine		c_{YWDEi}	u_{YWDEi}		
Calibration sensor mounting position uncertainty	B	1	u_{YWD3i}	1	b,c
Calibration maximum bin averaged wind direction difference due to wind direction	B	1	u_{YWD4i}	2	b,c
Calibration maximum bin averaged wind direction difference due to non-vertical flow	B	1	u_{YWD5i}	2	b,c
Sensor alignment	B	1	u_{YWD6i}	2	b,c
Rotor effect on measured yaw error	B	1	u_{YWD7i}	0	b,c
Data acquisition system	B	1	u_{dYWD2i}	0.1	b,c
Nacelle wind speed at yawed turbine		c_{YNi}	u_{YNi}		g
Calibration uncertainty due to wind speed	B	0.01	u_{YN1i}	0.15	b,c
Calibration uncertainty due to wind direction	B	0.01	u_{YN2i}	$0.01V_i$	b,c
Operational characteristics	B	0.01	u_{YN3i}	$0.12 + 0.012V_i$	b,c
Mounting effects	B	0.01	u_{YN4i}	$0.02V_i$	b,c
Data acquisition system	B	0.01	u_{dYNi}	0.03	b,c
Method					
Seasonal variation on WDTF	B	1	u_{MWDTFi}	0.6	b,d
Transfer function					
Variance in WDTF	A	1	s_{WDTFi}	1	b,e
Notes					
a: as in IEC61400-12-2:2013, Annex F&G					
b: newly defined component					
c: Same value chosen as for corresponding component for unyawed turbine					
d: based on 2% value for NTF in IEC61400-12-2:2013, but here with respect to max yaw error of 30 deg					
e: estimated using measurement data from Sedini wind farm					
g: the sensitivity value is a guess. In Example 3 no dependency on the wind speed was observed					
h: value in IEC61400-12-2:2013 is here slightly reduced due to improved calibration process					

Uncertainty in the WDTF measurement

For the uncertainty in the WDTF, similar approach is followed as for the WSTF above. The WDTF relates the measurement of the wind direction at an intentionally yawed turbine to that of a normally operating turbine. To construct the WDTF, measurements on two turbines close to each other, both operating in free stream, are required. The wind direction must be measured on both turbines (consisting of individual measurements of the nacelle positions and nacelle yaw errors). Furthermore, it may prove to be necessary to measure the wind velocity at the yawed turbine should it become clear in the future that the WDTF is significantly affected by parameter. Notice that in Example 3 no dependency on the wind speed was observed when an iSpin device is used for the measurement of the yaw error, but it still needs to be investigated whether this also holds when using the conventional measurement equipment located behind the blades.

The combined WDTF uncertainty is then

$$u_{WDTF,i} = \sqrt{u_{WDPi}^2 + u_{YWDPi}^2 + u_{WDEi}^2 + u_{YWDEi}^2 + u_{YNi}^2 + u_{MWDTFi}^2 + s_{WDTFi}^2} \tag{4.31}$$

wherein the combined uncertainties of the new components (not yet defined above) are given by the expressions

$$\begin{aligned} u_{WDPi} &= \sqrt{c_{WDPi}^2 u_{WD1i}^2 + c_{WDPi}^2 u_{WD2i}^2 + c_{WDPi}^2 u_{dWD1i}^2} \\ u_{YWDPi} &= \sqrt{c_{YWDPi}^2 u_{YWD1i}^2 + c_{YWDPi}^2 u_{YWD2i}^2 + c_{YWDPi}^2 u_{dYWD1i}^2} \\ u_{WDEi} &= \sqrt{c_{WDEi}^2 \left(\sum_{k=3}^{7} u_{WDki}^2 \right) + c_{WDEi}^2 u_{dWD2i}^2} \end{aligned}$$

Uncertainty in the consensus wind speed and consensus wind direction

The AWC validation methodology relies on the determination of a consensus wind speed V_{cons} and consensus wind direction $\alpha_{WD,cons}$. These are determined using the available measurements at the turbines in free stream operation (see last paragraphs of sections 4.1 and 4.2).

The consensus wind speed requires measurements of the nacelle wind speed and nacelle yaw error, which are fed into the WSTF compensate for the effect from yaw misalignment on the wind speed measurement. Only upstream turbines operating in free stream conditions are used to construct the consensus wind speed by means of averaging. The number of such turbines, N_j, depends on the wind direction due to the wind farm layout. Table 4 lists the uncertainty components for the consensus wind speed for a given bin (i, j), represented by the bin median wind velocity V_i and wind direction α_j. These components can also be found in the IEC61400-12-2:2013 standard, with the exception of the subcomponent “combined uncertainty on WSTF”, which is new here. Notice that the sensitivity parameters are inversely proportional to the number of turbines N_j that participate in the determination of the consensus wind speed. This is due to the averaging operation involved. The values in the numerator of the sensitivity parameters are equivalent to those for the corresponding components in Tables 2 and 3. Notice that even though the magnitude for these uncertainty components are chosen the same as those in Tables 2 and 3, in practice their values can differ since the WSTF and WDTF can be measured at a different site under different atmospheric conditions. For that reason, different notation is used here to clearly distinguish between these measurements. Finally, it should be stressed that the uncertainty components listed in Table 4 are for a single turbine from the set of N_j free stream turbines participating in the determination of the consensus wind speed.

These turbine-wise uncertainties will first be consolidated to construct combined uncertainties per bin. To this end, denote $s_{c,b,t}$ and $u_{c,b,t}$ as the uncertainty from A or B category, respectively, for component c on turbine t in bin b. Under the simplifying assumptions in IEC 61400-12-2:2013 [2, p. 87], the collective uncertainties (including all turbines) are

$$s_{c,b}^2 = \sum_{t=1}^{N_j} s_{c,b,t}^2 \tag{4.32}$$

$$u_{c,b}^2 = \sum_{t=1}^{N_j} u_{c,b,t}^2 + 2 \sum_{t_1=1}^{N_j-1} \sum_{t_2=t_1+1}^{N_j} u_{c,b,t_1} u_{c,b,t_2} \rho_{c,t_1,t_2} \tag{4.33}$$

When the turbines are all of the same type, their uncertainty components are considered of the same magnitude, so that

$$\begin{aligned} s_{c,b,t_2} &= s_{c,b,t_1} \\ u_{c,b,t_2} &= u_{c,b,t_1} \\ \rho_{c,t_1,t_2} &= \rho_{c,t_1,t_1}, \end{aligned}$$

the expressions in equations (4.32) and (4.33) simplify to

$$s_{c,b}^2 = N_j s_{c,b,1}^2 \tag{4.34}$$

$$\begin{aligned} u_{c,b}^2 &= N_j u_{c,b,1}^2 + (N_j^2 - N_j) u_{c,b,1}^2 \rho_{c,1,1} \\ &= N_j \left(1 + \rho_{c,t_1,t_1}(N_j - 1)\right) u_{c,b,1}^2 \end{aligned} \tag{4.35}$$

Now that expressions are obtained for the collective uncertainties for all N_j turbines participating in the determination of the consensus wind speed, the combined uncertainty in the consensus wind speed can be written using these relations

$$u_{ConWS,ij} = \sqrt{c_{Vj}^2 u_{Vi}^2 + c_{YEj}^2 u_{YEi}^2} \tag{4.36}$$

where

$$\begin{aligned} u_{Vi} &= \sqrt{u_{dVi}^2 + \sum_{k=1}^{6} u_{Vki}^2} \\ u_{YEi} &= \sqrt{u_{dD2i}^2 + \sum_{k=3}^{7} u_{Dki}^2}. \end{aligned}$$

For the consensus wind direction, similar argumentation is used. The list of uncertainty components identified in this case are given in Table 5, which are now related to the measurements of the wind direction (nacelle position and yaw error) and wind velocity at the N_j upstream turbines operating in free stream. The general-form expressions in equations (4.34) and (4.35) are applicable here as well to merge the individual turbines' uncertainties into collective uncertainties, before constructing the combined uncertainty for the consensus wind direction given by the equation

$$u_{ConWD,ij} = \sqrt{c_{Vj}^2 u_{Vi}^2 + c_{YPj}^2 u_{YPi}^2 + c_{YEj}^2 u_{YEi}^2} \tag{4.37}$$

where

$$u_{YPi} = \sqrt{u_{dD1i}^2 + u_{D1i}^2 + u_{D2i}^2}.$$

Table 4: Uncertainty components for the Consensus wind speed

Uncertainty component	Cat.	Sens.	Notation	Magnitude	Note
Nacelle wind speed at turbine $t = 1..N_j$		c_{Vj}	u_{Vit}	$[m/s]$	
Calibration uncertainty due to wind speed	B	$1/N_j$	u_{V1it}	0.15	a
Calibration uncertainty due to wind direction	B	$1/N_j$	u_{V2it}	$0.01V_i$	a
Operational characteristics	B	$1/N_j$	u_{V3it}	$0.12 + 0.012V_i$	a
Mounting effects	B	$1/N_j$	u_{V4it}	$0.02V_i$	a
Flow distortion due to terrain	B	$1/N_j$	u_{V5it}	$0.01V_i$	a,c
Combined uncertainty on WSTF	A,B	$1/N_j$	u_{V6it}	$u_{WSTF,i}$	b
Data acquisition system	B	$1/N_j$	u_{dVit}	0.03	a
Nacelle yaw error at turbine $t = 1..N_j$		c_{YEj}	u_{YEit}	$[deg]$	
Calibration sensor mounting position uncertainty	B	$0.05/N_j$	u_{D3it}	1	a
Calibration maximum bin averaged wind direction difference due to wind direction	B	$0.05/N_j$	u_{D4it}	2	a
Calibration maximum bin averaged wind direction difference due to non-vertical flow	B	$0.05/N_j$	u_{D5it}	2	a
Sensor alignment	B	$0.05/N_j$	u_{D6it}	2	a
Rotor effect on measured yaw error	B	$0.05/N_j$	u_{D7it}	0	a
Data acquisition system	B	$0.05/N_j$	u_{dD2it}	0.1	a
Notes					
a: as in IEC61400-12-2:2013, Annex F&G					
b: newly defined component					
c: chosing terrain class 1					

Uncertainty in the wind farm power production

The uncertainty in the farm power production is related to the electric power measurement at the individual wind turbines, the consensus wind speed and direction measurements used in the process of binning, and the statistical uncertainty in the farm electric power. These are all listed in Table 6, including their subcomponents, their magnitudes and sensitivity coefficients. Much of these components have directly been adopted from the IEC 61400-12-2:2013 standard. The table also includes some uncertainty components, related to the method, although their values are set to zero as they are considered to have an insignificant contribution to the uncertainty. The seasonal effects, for instance, are considered irrelevant when the test campaign duration is one year or longer and the toggle period is much smaller than the duration of a season. Since all turbines are of the same type and the method is meant for performing site-specific analysis only, the effects from rotor inflow variation and turbulence on the binning are neglected.

The combined uncertainty for the wind farm power production in bin $b = (i, j)$, represented by median wind velocity V_i and wind direction α_j is then

$$u_b = \sqrt{c_{Pij}^2 u_{Pij}^2 + c_{Wsij}^2 u_{Wsij}^2 + c_{Wdij}^2 u_{Wdij}^2 + c_{Mij}^2 u_{Mij}^2 + s_{Pij}^2} \tag{4.38}$$

where

$$\begin{aligned} u_{Pij} &= \sqrt{u_{dPij}^2 + \sum_{k=1}^{3} u_{Pkij}^2}. \\ u_{Mij} &= \sqrt{\sum_{k=5}^{7} u_{Mkij}^2}. \end{aligned}$$

Table 5: Uncertainty components for the Consensus wind direction

Uncertainty component	Cat.	Sens.	Notation	Magnitude	Note
Nacelle wind speed at turbine $t = 1..N_j$		c_{Vj}	u_{Vit}	$[m/s]$	
Calibration uncertainty due to wind speed	B	$0.01/N_j$	u_{V1it}	0.15	a
Calibration uncertainty due to wind direction	B	$0.01/N_j$	u_{V2it}	$0.01V_i$	a
Operational characteristics	B	$0.01/N_j$	u_{V3it}	$0.12 + 0.012V_i$	a
Mounting effects	B	$0.01/N_j$	u_{V4it}	$0.02V_i$	a
Flow distortion due to terrain	B	$0.01/N_j$	u_{V5it}	$0.01V_i$	a,c
Data acquisition system	B	$0.01/N_j$	u_{dVit}	0.03	a
Nacelle yaw position at turbine $t = 1..N_j$		c_{YPi}	u_{YPit}	$[deg]$	
Calibration	B	$1/N_j$	u_{D1it}	2.5	a,h
Signal resolution	B	$1/N_j$	u_{D2it}	0.5	a
Data acquisition	B	$1/N_j$	u_{dD1it}	0.1	a
Nacelle yaw error at turbine $t = 1..N_j$		c_{YEi}	u_{YEit}	$[deg]$	
Calibration sensor mounting position uncertainty	B	$1/N_j$	u_{D3it}	1	a
Calibration maximum bin averaged wind direction difference due to wind direction	B	$1/N_j$	u_{D4it}	2	a
Calibration maximum bin averaged wind direction difference due to non-vertical flow	B	$1/N_j$	u_{D5it}	2	a
Sensor alignment	B	$1/N_j$	u_{D6it}	2	a
Rotor effect on measured yaw error	B	$1/N_j$	u_{D7it}	0	a
combined uncertainty on WDTF	A,B	$1/N_j$	u_{D8it}	$u_{WDTF,i}$	b
Data acquisition system	B	$1/N_j$	u_{dD2it}	0.1	a
Notes					
a: as in IEC61400-12-2:2013, Annex F&G					
b: newly defined component					
c: chosing terrain class 1					
c: h: value in IEC61400-12-2:2013 is here slightly reduced due to improved calibration process					

To calculate the uncertainty on the power ratio within a given bin b, as defined in equation (4.20), the combined uncertainties per bin for the two test conditions (nominal and controlled) need to be first calculated. Denoting $u_b^{(1)}$ as the total uncertainty on the wind farm power production $\bar{P}_{b,farm}^{(1)}$ within bin $b = (i, j)$ under the controlled test scenario (with AWC active), and $u_b^{(2)}$ as its counterpart ($\bar{P}_{b,farm}^{(2)}$) under nominal operating conditions, and assuming independence between the two, it can easily be shown (using, e.g., the formulas in [5]) that the following expression holds for the uncertainty on the power ratio

$$u_{dP,b} = \sqrt{\left(\frac{1}{\bar{P}_{b,farm}^{(2)}}\right)^2 \left(\left(u_b^{(1)}\right)^2 + \left(\widehat{\delta P}_b\right)^2 \left(u_b^{(2)}\right)^2\right)}. \tag{4.39}$$

Finally, an expression will be obtained for the uncertainty on the weighted power ratio, defined in equation (4.27). To this end, it is necessary to distinguish between the contribution of the A and B category components on the wind farm power production per bin for each test condition. Denote $s_b^{(1)}$ and $s_b^{(2)}$ be the combined A category uncertainties for bin b for the test conditions with and without AWC, respectively, and $u_{B,b}^{(1)}$ and $u_{B,b}^{(2)}$ be their B category counterparts. For the A and B category uncertainties in the weighted power productions in the two test cases, $\sum_{b=1}^{B} \alpha_b P_{b,farm}^{(s)}$, $s = 1, 2$, the

Table 6: Uncertainty components for the wind farm power production

Uncertainty component	Cat.	Sens.	Notation	Magnitude	Note
Power output at turbine i ($i = 1..N$)		c_{Pij}	u_{Pij}	$[W]$	
Current transformers	B	1	u_{P1ij}	$0.75\%P_i$	a
Voltage transformers	B	1	u_{P2ij}	$0.5\%P_i$	a
Power transducer or measurement device	B	1	u_{P3ij}	$0.5\%P_i$	a
Data acquisition	B	1	u_{dPij}	$0.1\%P_i$	a
Wind conditions for binning			u_{Wij}		
Combined uncertainty on Consensus WS	A,B	$\left\|\frac{P_i-P_{i-1}}{V_i-V_{i-1}}\right\|$	u_{Wsij}	u_{CWS}	b
Combined uncertainty on Consensus WD	A,B	$\left\|\frac{P_j-P_{j-1}}{\alpha_j-\alpha_{j-1}}\right\|$	u_{Wdij}	u_{CWD}	b
Method		c_{Mij}	u_{Mij}		
Seasonal effects	B	1	u_{M5ij}	0	a,i
Variation rotor inflow	B	1	u_{M6ij}	0	a,j
Turbulence effect on binning	B	1	u_{M7ij}	0	a,j
Statistical uncertainty contributions					
Electric power variation	A	1	s_{Pij}	$std/sqrt(L)$	a
Notes					
a: as in IEC61400-12-2:2013, Annex F&G					
b: newly defined component					
i: irrelevant when the test duration is 1 year or longer					
j: not relevant for site-specific analysis					

following expressions are in line with the approach in IEC 61400-12-2:2013

$$s^{(s)} = \sqrt{\sum_{b=1}^{B} \alpha_b^2 \left(s_b^{(s)}\right)^2},\ s = 1,2 \tag{4.40}$$

$$u_B^{(s)} = \sum_{b=1}^{B} \alpha_b u_{B,b}^{(s)},\ s = 1,2 \tag{4.41}$$

$$u^{(s)} = \sqrt{\left(u_B^{(s)}\right)^2 + \left(s^{(s)}\right)^2},\ s = 1,2 \tag{4.42}$$

For the combined uncertainty on the weighted power ratio (4.27) the following relation then follows

$$u_{dP} = \sqrt{\left(\frac{1}{\bar{P}_{av,farm}^{(2)}}\right)^2 \left(\left(u^{(1)}\right)^2 + \left(\widehat{\delta P}_{av}\right)^2 \left(u^{(2)}\right)^2\right)}. \tag{4.43}$$

Example 7 (Uncertainty analysis for offshore wind farm Westermost Rough)

To illustrate the uncertainty assessment methodology, it is applied to the measurement data from the Westermost Rough offshore wind farm, which was used earlier in Example 5 for the purpose of power ratio analysis. As a starting point, the magnitudes of the different uncertainty components listed in Tables 2, 3, 4, 5, and 6 are used. As mentioned in the beginning of this section, most of these numbers (the B category uncertainties, in particular) have been adopted from the examples in Annex G in the IEC61400-12-2:2013 standard [2]. They are not necessarily representative for this

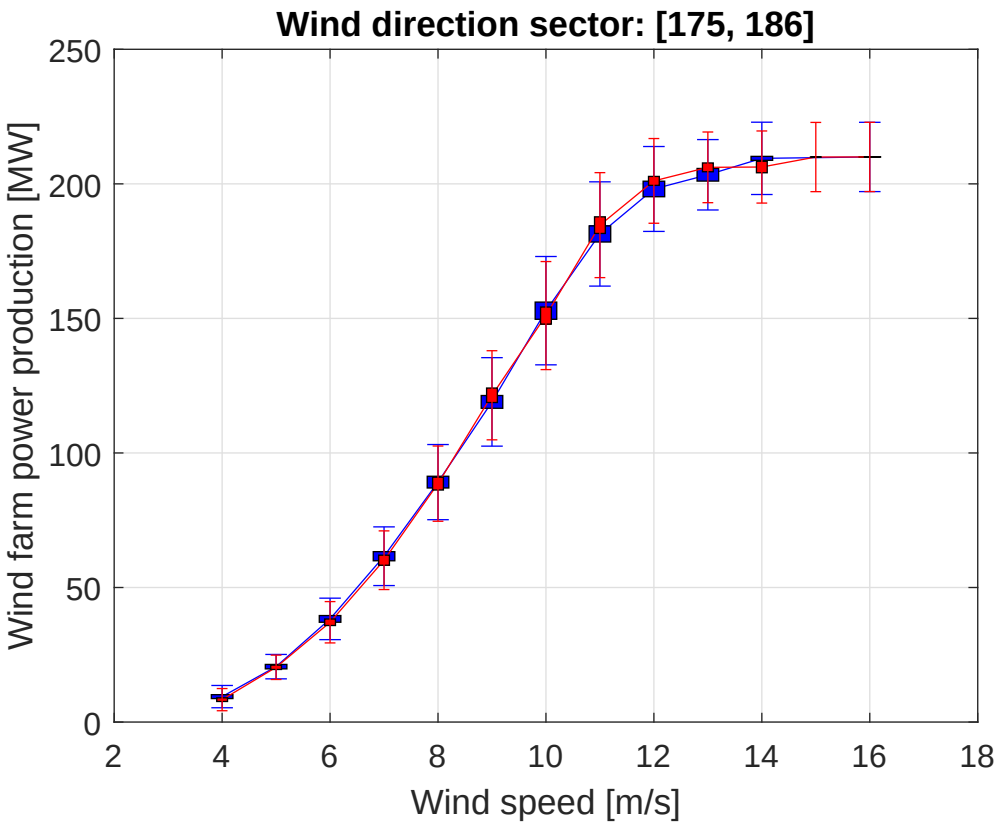

Figure 24: Uncertainty on the power curves for the Westermost Rough wind farm, wind direction sector 175° to 186°. The blue and red colors correspond to the two data sets, the thick bars represent the A category uncertainty, while the line segments depict the combined (A and B cat.) uncertainty.

specific case study, and are only meant to serve an illustrative purpose here. The A category uncertainties, on the other hand, have been calculated in this study using measurement data.

The A and B category uncertainties, as well as the combined uncertainty, have first been calculated per bin for each of the two data sets (see Example 5 for more information regarding the data sets and the binning process). Figures 24 and 25 depict the power curves for the two data sets (given in blue and red) and for wind direction sectors of 175° to 186° and 267° to 279°, respectively. The A category uncertainty is depicted by the thick blue and red bars, while the blue and red vertical line segments represent the combined (A and B category) uncertainty. Clearly, the overall uncertainty is largely dominated by the B category uncertainty.

Next, the uncertainty on the power ratio per bin has been computed, and plotted in Figure 26 for the different wind direction sectors. The wind speed dependency has been removed by applying weighted averaging over the wind speeds up to 13 m/s using the measured frequency distribution of the wind speed. The light shaded bars represent the combined (A and B category) uncertainty, while the dark shaded ones – the contribution of the A category uncertainty. The red segment lines are the mean values per wind direction sector. Also here the earlier conclusion of the B category uncertainties being dominant is apparent.

Finally, the uncertainty on the average power ratio, defined in equation (4.27)*, has been calculated to be close to 17 %. The A category uncertainty is responsible for just about 0.3 %.*

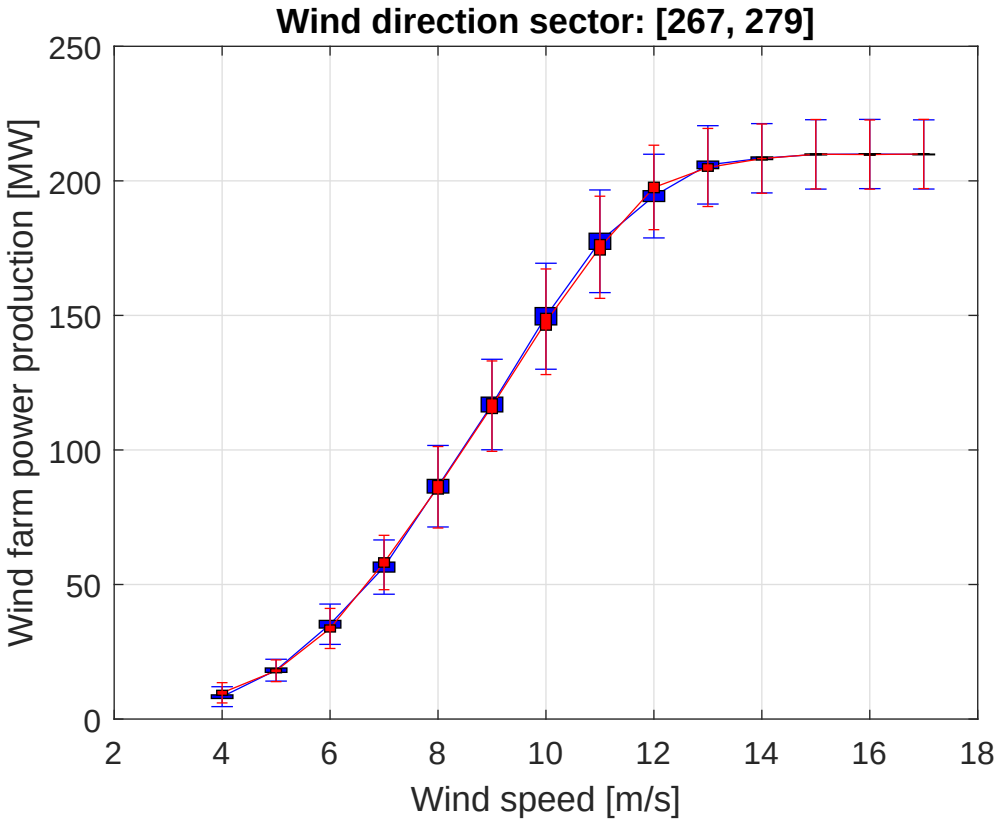

Figure 25: Uncertainty on the power curves for the Westermost Rough wind farm, wind direction sector 267° to 279°. The blue and red colors correspond to the two data sets, the thick bars represent the A category uncertainty, while the line segments depict the combined (A and B cat.) uncertainty.

Example 8 (Uncertainty analysis for offshore wind farm Anholt)

As a second illustration of the the uncertainty assessment methodology, the measurement data from offshore wind farm Anholt is used. These data was introduced in Example 4 where it was used for power ratio analysis. The uncertainty analysis, performed here, is analogous with the one described in Example 7 above and, therefore, the details will be omitted here to avoid repetition.

Figures 27 and 28 depict the power curves for the two data sets (given in blue and red) and for wind direction sectors of 175° to 184°, and 259° to 271°, respectively. The A category uncertainty is depicted by the thick blue and red bars, while the blue and red vertical line segments represent the combined (A and B category) uncertainty. Similarly to the conclusions made in Example 7, the overall uncertainty is dominated by the B category uncertainty.

Next, the uncertainty on the power ratio per bin is given in Figure 26 for the different wind direction sectors. Again, the overall uncertainty is primarily determined by the category B uncertainty.

Finally, the uncertainty on the average power ratio is nearly 20 %. The A category uncertainty is responsible for just about 0.3 %.

The most important conclusions from above two examples of the uncertainty analysis are as follows:

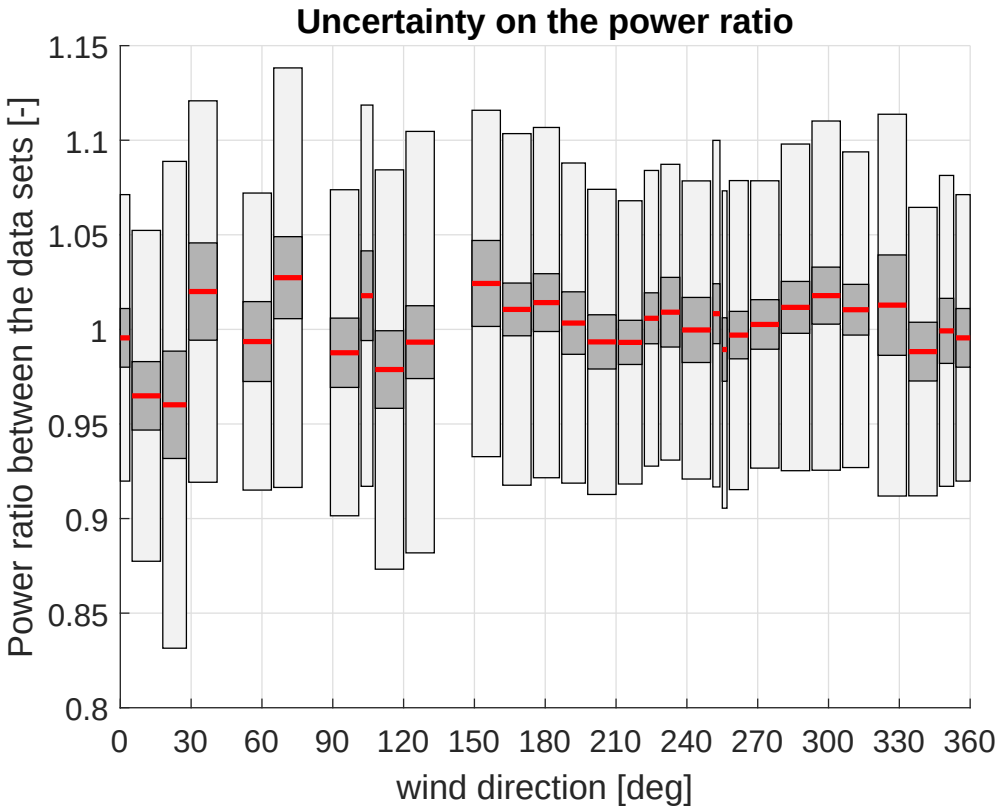

Figure 26: Uncertainty on the power ratio per wind direction sector for the Westermost Rough wind farm. The dark shaded bars represent the A category uncertainty, the light shaded bars – the combined (A and B cat.) uncertainty, and the red lines – the mean values.

- Category B uncertainties represent the dominant source of uncertainty at all stages in the AWC analysis: the wind farm power production per bin, the power ratio per bin, and the average power ratio.
- Category B uncertainties are not influenced by the bin sizes. Making the wind direction sectors wider influences the A category uncertainty as the number of measurement data points that fall within a bin changes, but not the B category uncertainty that only depends on the median wind speed and direction for a given bin.
- The calculated category B uncertainties in the examples intuitively seem too large. For instance, for wind velocities above 14 m/s the B category uncertainty is above the 6 %, which results from the aggregation of the B uncertainties of the 35 individual turbines (which are in the order of 1 % each and are assumed mutually independent).
- The power curves calculated for the two data sets match quite well, which is expected as the two data sets come from the same test case (nominal operation) in both examples. This indicates that, (a) the approach seems quite accurate and suggests that it should be possible to quantify the impacts of AWC on the power gain well enough given good quality data of sufficient length and, (b) suggests that the (B category) uncertainty margins seem quite conservative. In other words, given the relatively large uncertainty margins it is hardly conceivable that the power curves essentially lay on top of each other.

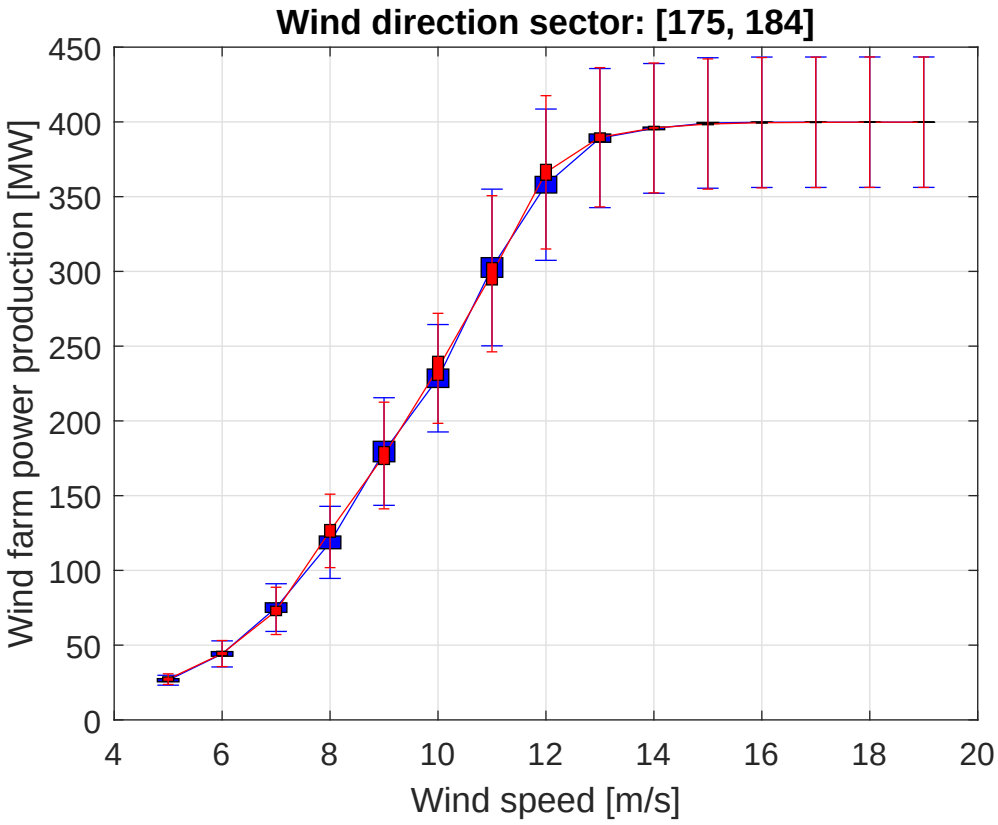

Figure 27: Uncertainty on the power curves for the Anholt wind farm, wind direction sector 175° to 184°. The blue and red colors correspond to the two data sets, the thick bars represent the A category uncertainty, while the line segments depict the combined (A and B cat.) uncertainty.

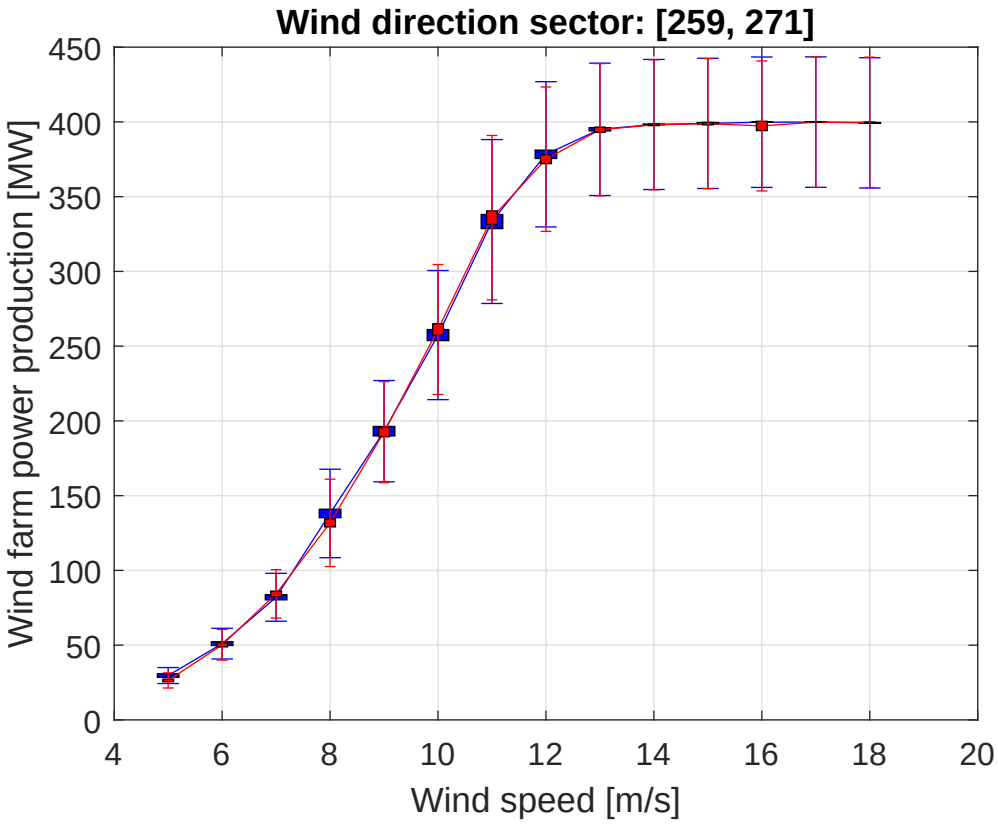

Figure 28: Uncertainty on the power curves for the Anholt wind farm, wind direction sector 259° to 271°. The blue and red colors correspond to the two data sets, the thick bars represent the A category uncertainty, while the line segments depict the combined (A and B cat.) uncertainty.

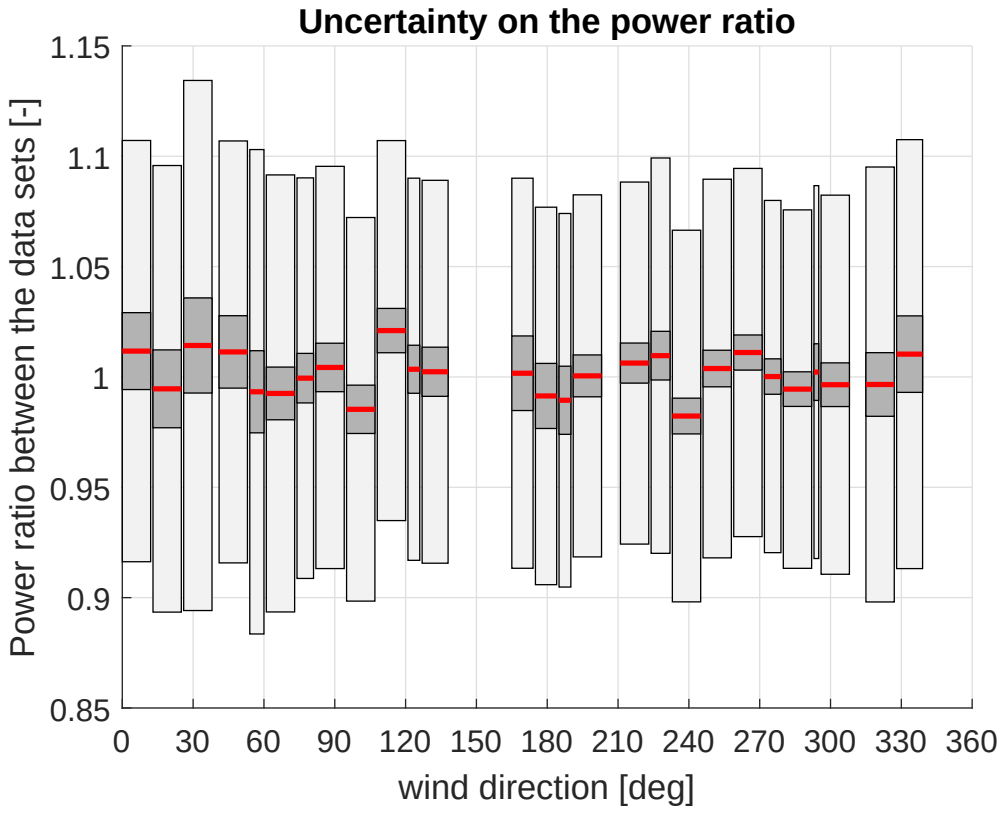

Figure 29: Uncertainty on the power ratio per wind direction sector for the Anholt wind farm. The dark shaded bars represent the A category uncertainty, the light shaded bars – the combined (A and B cat.) uncertainty, and the red lines – the mean values.

5 Summary of the AWC validation method

Section 4 above describes in detail the different components of the AWC validation methodology. In this section, the complete process is summarized in the form of a flow chart, depicted in Figure 30. The following points are important to note:

- The WSTF and WDTF can be either provided, or constructed. If provided, they need to be validated as explained in section 4.1 and 4.2. If they need to be constructed, this could either be done before the actual AWC test campaign starts, or during its execution, provided that this is carried out in a way that it does not interfere with the AWC testing. For instance, the WSTF and WDTF measurement can be performed in sectors of wind directions where AWC is not operational.
- During the preparation phase it is important to perform (software) calibration of the nacelle direction sensors as these are known to often exhibit bias that may change over time. During the analysis phase these calibration settings need to be verified periodically and, if needed, updated to ensure consistent measurements throughout the campaign.
- The data acquisition is to be performed by toggling AWC on and off at predefined periods of time (see also section 4.8). The goal is to ensure that a comparable amount of data records is collected for similar wind conditions.
- The data analysis includes verification/update of the nacelle direction calibration (see section 4.2), determination of consensus wind speed and wind direction (sections 4.1 and 4.2), data filtering (section 4.3), binning (section 4.4), and power ratio analysis (sections 4.7).
- The data analysis can be performed at certain periods of time (e.g. every 3 months) until the database requirements are fulfilled, i.e. until the normalized standard error of the wind farm power production, for each of the two data sets, gets below a certain value (e.g. 5 %) for all wind bins in which AWC applies.
- After the database requirements are fulfilled, a complete uncertainty analysis is performed and reported.

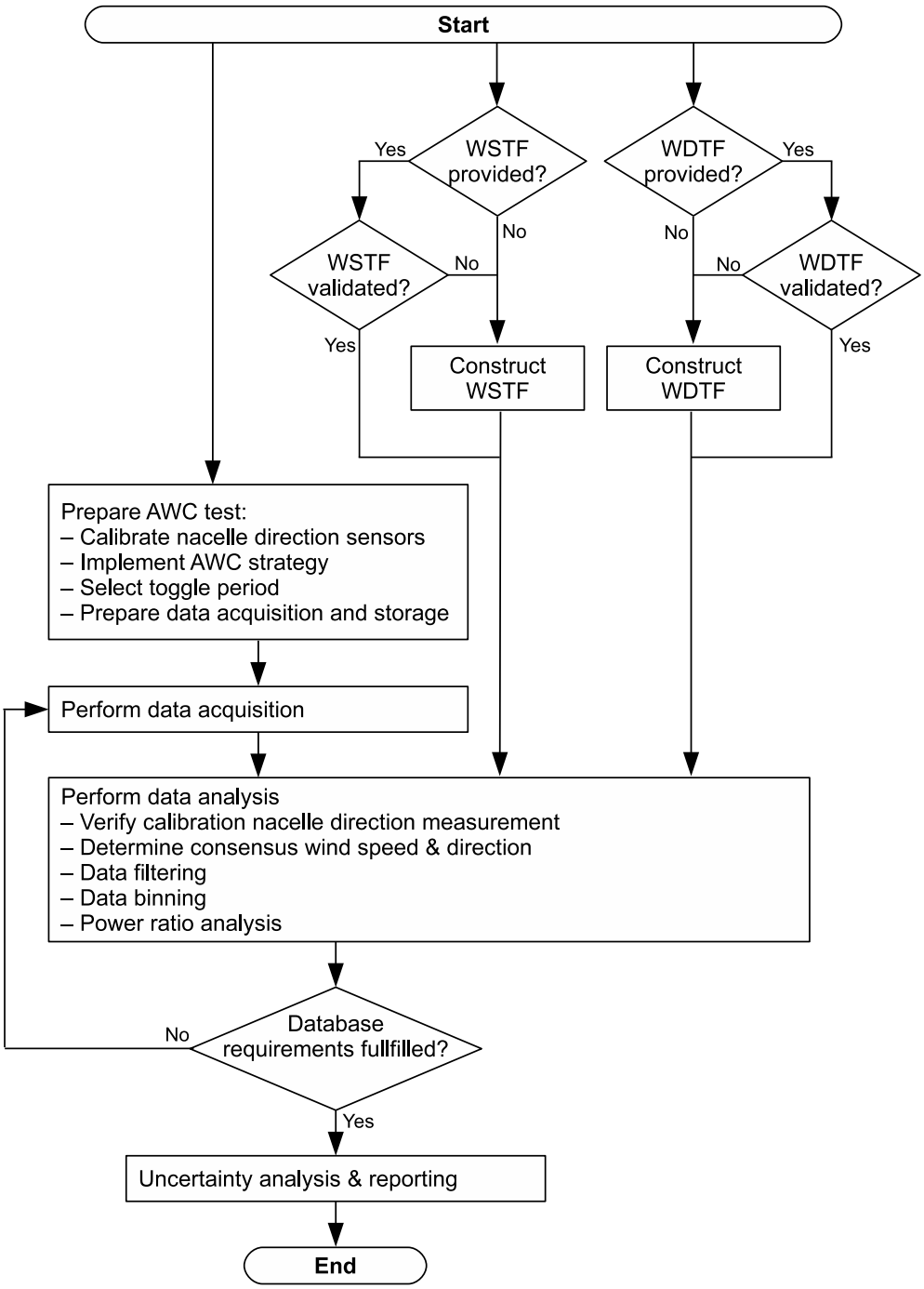

Figure 30: Flow chart of the AWC validation methodology

6 Conclusions and future work

This report describes the development of an AWC validation methodology, applicable to offshore wind farms of any size and layout, and using the conventionally available SCADA data only. The main conclusions from the study are as follows:

- In order to have consistent measurements of the wind speed and wind direction, WSTF and WDTF need to be constructed, or provided. These transfer functions model the effect of yaw misalignment onto the wind speed and yaw error measurements. The WSTF and WDTF are used by the AWC validation methodology to apply corrections to the measurements of the wind speed and yaw error at wind turbines operating under intentional yaw misalignment (i.e. in AWC mode), so as to make these measurements consistent to those during nominal operation.
- Consensus wind speed and consensus wind direction measurements, representative for the whole farm, are needed. These can be constructed by means of averaging the measurements (corrected by the WSTF and WDTF) at upstream wind turbines that operate in free stream, are available and not temporarily curtailed or power-boosted.
- Data records containing some unavailable wind turbines do not need to be filtered out as that could result in an insufficient amount of data points for proper statistical analysis. The developed approach can deal with data records containing missing measurements from some of the wind turbines.
- In order to allow for proper comparison between different data sets (test scenarios), the measurements are to be binned with respect to the consensus wind speed and consensus wind direction. The bin size needs to be carefully selected to ensure sufficient data per bin. To this end, it is recommended to keep the bin size for the wind speed at 1 m/s, and design wind direction bins of variable size to ensure that the uncertainty (standard error) remains below some selected threshold.
- The ambient atmospheric conditions, such as air density, turbulence intensity and wind shear, are not used in the AWC validation methodology as their measurement cannot be assumed available at every site (measurements inside the nacelle, or behind the rotor are not sufficient for this purpose).
- The AWC validation methodology has been illustrated with two case studies, including 2,5 years of 10-minute averaged SCADA data from the offshore wind farms Westermost Rough and Anholt. Both wind farms have been operated nominally (no AWC involved). In order to apply the validation method, in each case study the available measurement data has been divided into two parts, with the intention to verify if the calculated power ratio is close to unity. In both examples, the AWC validation methodology delivered highly accurate results when comparing the results from the two data sets in each example: marginal differences in the power curves, and on average close to unity power ratios for each bin.
- The toggling between the two test conditions (nominal and with AWC) should be ideally done at a period of 2 to 3 hours, to ensure best results in terms of mean power ratio and its uncertainty. If such high toggle rate is prohibitive (for instance, due to the resulting yaw duty), a toggle period between 1 day and 1 week should be selected, but kept as short as possible. Toggle periods between 3 hours and 1 day are not recommended as diurnal cycle phenomena may bias the results.

- A detailed uncertainty analysis method is developed and illustrated with the Westermost Rough and Anholt data. The category A uncertainty is calculated using the measurement data provided. The values used for category B uncertainties, however, have largely been adopted from the IEC 61400-12-2:2013 standard, and are therefore not specific for the turbines at the sites considered. Nevertheless, it becomes clear from the examples that category B uncertainties represent the dominant source of uncertainty at all stages in the AWC analysis. These uncertainties are primarily related to the hardware and software used for collecting and storage of the measurement data, and are hence rather independent of the AWC validation method itself.

In the near future, the developed AWC validation methodology is intended to be applied to measurement data from full-scale test campaigns with AWC by wake redirection. This will certainty give rise to new insights and lead to further refinements of the methodology. More specifically, important and critical components to verify using relevant field data are the WSTF and WDTF. These could not be verified using the available (nominal operation) data, while their accuracy is critical for obtaining reliable power ratio estimates.

7 Bibliography

[1] *Wind energy generation systems – Part 12-1: Power performance measurements of electricity producing wind turbines (IEC 61400-12-1:2015)*. International Electrotechnical Commission. Mar. 2017.

[2] *Wind turbines – Part 12-2: Power performance of electricity-producing wind turbines based on nacelle anemometry (IEC 61400-12-2:2013)*. International Electrotechnical Commission. Mar. 2013.

[3] N. Mittelmeier and M. Kühn. “Determination of optimal wind turbine alignment into the wind and detection of alignment changes with SCADA data.” In: *Wind Energy Science* 3 (2018), pp. 395–408. DOI: 10.5194/wes-3-395-2018.

[4] E.T.G. Bot and S. Kanev. *FarmFlow: extensively validated and dedicated model for wind farm control*. Tech. rep. TNO, 2020. URL: http://publications.tno.nl/publication/34636587/0U5yUJ/Bot-2020-Farmflow.pdf.

[5] H.H. Ku. “Notes on the use of propagation of error formulas.” In: *Journal of research of the National Bureau of Standards – C. Engineering and Instrumentation* 70C.4 (1966), pp. 263–273.